Equivalent frame idealization of walls with irregular openings in masonry buildings

Equivalent frame idealization of walls with irregular openings in masonry buildings

Serena Cattari[1,*], Antonio Maria D'Altri[2], Daniela Camilletti[1], Sergio Lagomarsino[1]

[1] DICCA, Dept. of Civil, Chemical Environmental Engineering, University of Genova, Via Montallegro 1, Genova, 16145, Italy

[2] DICAM, Dept. of Civil, Chemical, Environmental and Materials Engineering, University of Bologna, Viale del Risorgimento 2, Bologna, 40136, Italy

*Corresponding Author, serena.cattari@unige.it

ABSTRACT: Within the framework of modelling of unreinforced masonry structures, the equivalent frame (EF) approach is widely used for the seismic assessment. However, the definition of modelling rules for the EF idealization of walls is not always straightforward. Such rules are typically applied *a priori* and they can strongly affect the seismic response. This paper aims to investigate the reliability of four existing rules for the *a priori* identification of the geometry of the piers, i.e. the elements in charge of resisting the horizontal and vertical loads. This constitutes the first main issue within the EF idealization of walls. Continuum finite element (FE)-based numerical solutions are considered as reference to assess the reliability of EF approach for a number of irregular masonry walls case studies. The investigated irregularity deals with the presence of openings with different height at the same storey or the presence of small openings. The critical comparison between FE and EF solutions is made in terms of (i) pushover curves, (ii) damage patterns, (iii) generalized forces, and (iv) drift values at scale of single elements. The results herein achieved allow to provide practical recommendations for EF walls idealization. In particular, some existing rules for the *a priori* identification of the geometry of the piers already appeared to work properly, while specific precautions appeared to be needed for other rules or in specific cases, which have been identified. More specifically, the rules that may lead to very squat piers appeared to be particularly problematic since may produce a significant underestimation of the ultimate displacement capacity at least when compared to the one estimated by the FE model, assumed as reference solution in the paper. Finally, in the case of small openings, results suggest how the most reliable solution consists of neglecting them in the EF idealization process. To support analysts in this choice, some preliminary indications on the dimensions that identify "small openings" are also provided in the paper.

KEYWORDS: Equivalent frame model, Irregular opening layout, Pier geometry, Nonlinear static analyses, Finite element model

1. INTRODUCTION

The assessment of the seismic vulnerability of existing unreinforced masonry (URM) buildings is a relevant issue, typically addressed through numerical models (Lourenço 2002, Roca et al. 2010, D'Altri et al. 2019). In this context, several numerical modelling strategies have been developed for masonry structures in the last decades, adopting different hypotheses and different scales of representation, i.e. from masonry blocks (e.g. Petracca et al. 2017, Angiolilli et al. 2021, Mercuri et al. 2021) to masonry

homogenised material (e.g Milani (2011), Silva et al. (2020)) or directly to masonry panels (e.g. Magenes and della Fontana (1998), Lagomarsino et al. (2013), Vanin et al. (2020)). In this framework, the equivalent frame (EF) modelling approach plausibly represents the most diffused, also explicitly recommended by several national and international codes (NTC18 (2018), Eurocode 8 (CEN (2005), NZSEE (2017)). This approach assumes that the nonlinear response of each wall is concentrated in specific masonry panels which are defined *a priori*, namely: the piers, vertical panels; and the spandrels, masonry beams that connect piers. The remaining portions of the masonry wall are typically idealized as rigid nodes. This hypothesis is consistent with typically observed seismic-induced damage patterns. In fact, cracks often appear in masonry portions located between the openings aligned in the horizontal (for piers) and vertical (for spandrel) direction. At present, this approach is substantially oriented to the analysis of ordinary or strategic URM buildings, which are indeed the subject of this paper. Its application to monumental buildings (e.g. churches, mosques, fortresses, etc.), although with some successful examples (e.g. in Rossi et al. 2015, Torres et al. 2019), has to be carefully adopted due to the difficulties in identifying piers and spandrels in complex geometries.

Despite of the widespread use of EF models, several specific aspects have not been validated yet in a robust way and seismic codes generally do not provide detailed indications about EF idealization choices. Typically, some arbitrary choices could arise in the identification of structural elements, the modelling of diaphragms and the flange effect, the effective length of the reinforced concrete (r.c.) tie beams, to name a few (as debated for example in Bracchi et al. 2015, Quagliarini et al. 2017, Cattari et al. 2021a). All of these issues could have a remarkable impact on the seismic assessment results and on the scatter of achievable results (Marques and Lourenço (2011), Calderoni et al (2015), De Falco et al (2017), Aşıkoğlu et al. (2020), Bartoli et al. (2017), Esposito et al. (2019), Parisse et al. (2021)). For these reasons, for example, the *URM nonlinear modelling*—Benchmark research project (Cattari and Magenes 2021) recently attended to quantify such a dispersion by comparing the results obtained on benchmark study cases analysed through different software packages (Ottonelli et al. 2021, Manzini et al. 2021, Castellazzi et al. 2021).

Within this manifold topic, in this paper, the attention is focused on the problem of the *a priori* identification of the geometry of the piers. In particular, the issue essentially involves the so called

"effective height" of piers (h_{eff}), i.e. the height of the element in which the nonlinearity is concentrated to, typically lower that the actual inter-storey height.

The existing criteria commonly used to this aim are mainly related to the opening layout of the considered wall. In the case of *regular openings layouts,* the identification of the frame structural components is generally straightforward. However, no international level rules are recognized and available for masonry walls and the conventionality in the application of available rules increases with *irregular openings layouts* (Asıkoglu et al. 2021).

A systematic classification of the most recurrent types of irregularities that can affect masonry walls has been firstly provided by Parisi and Augenti (2013). Particularly, four basic irregularity types have been identified: (1) *horizontal irregularity*, i.e. walls characterized by openings with different heights at the same story and equal widths along the height; (2) *vertical irregularity*, i.e. walls characterized by openings with equal heights at the same story and different widths along the height; (3) *offset irregularity*, i.e. when a wall presents horizontal and/or vertical offsets between openings with equal or different sizes; (4) *variable openings number irregularity*, i.e. walls with different number of openings per story. Other more recent research works (Berti et al (2017), Siano et al (2017a), Siano et al (2017b)) considered the effects produced by the irregularities on the accuracy of the EF modelling approach. In particular, the comparison with more accurate modelling techniques (e.g. continuum FE and block-based approaches), considered as reference solution, has been carried out. Although these research works represent a first attempt to evaluate the reliability of the EF application to irregular masonry walls, the outcomes are not fully exhaustive as the comparisons with reference solutions are limited to global responses and qualitative checks on the damage pattern, without providing specific practical indications. Accordingly, a systematic and in-depth analysis considering also local response is still lacking.

In this paper, the reliability of four existing rules for the a priori identification of the geometry of piers is investigated, namely those proposed by: Dolce (1991), Lagomarsino et al. (2013), Moon et al. (2006) and Augenti (2006). The relevance of the modelling uncertainty resulting from the application of such four rules has been recently proven in Manzini et al. (2021) and Ottonelli et al. (2021) for 3D URM structures, consisting of a 2-storey single unit URM building and a complex building with irregular T-shape plan. In both cases, the opening layout of walls was quite regular. Conversely, in this paper, they

are applied to 2D masonry walls with *irregular* opening layout. Despite the oversimplification made by 2D models with respect to 3D actual structures, it allows to focus only on how the EF idealization process affects the capability of the model to correctly reproduce the in-plane response of URM walls, which is one of basic steps of this modelling strategy. Of course, when 3D models are then assembled, piers are subjected also to other effects (such as the interaction with diaphragms or the flange effects) but the results obtained from the 2D model can be still considered valid (at least concerning their geometry). More specifically, the *irregular* opening layout analysed in the paper refers to the presence of openings with different heights at the same storey and the presence of small openings.

Continuum finite element (FE)-based numerical solutions, which assume masonry as an isotropic quasi-brittle material, are considered as reference target. Basically, the methodological approach adopted and validated for regular masonry walls by the authors in Cattari et al. (2021b) is herein extended to irregular walls. Accordingly, a critical comparison between FE and EF solutions is carried out in terms of (i) pushover curves, (ii) damage patterns, (iii) generalized forces, and (iv) drift values at scale of single elements.

The paper is structured as follows. Section 2 describes the methodology adopted. Section 3 investigates and compares several possible choices for the pier geometry identification. Section 4 discusses the effects of the presence of small openings. Section 5 highlights the conclusions of this research work.

2. ADOPTED METHODOLOGY

2.1. Models employed in structural analyses

A continuum FE modelling approach, in which the masonry material is modelled as an equivalent isotropic continuum, is considered as reference solution to evaluate the effectiveness of the EF approach. Once defined the structure under study, the procedure herein adopted consists in: (i) the EF model idealization through different criteria available in the literature; (ii) the implementation of nonlinear static analyses (NLSA) on both EF and FE models; and (iii) the comparison of two modelling strategies, i.e. computing the difference of the EF solution with respect to the FE one. To this aim, two-storey masonry walls with openings characterized by a *strong spandrel-weak pier* behavior type are herein

considered as benchmarks. Indeed, the presence of an r.c. beam at the floor levels permits to focus the attention directly on the piers.

2.1.1. Equivalent frame model

EF model-based analyses are conducted through the Tremuri program (Lagomarsino et al. (2013)). URM panels are conceived as nonlinear beams with lumped inelasticity idealization according to the piecewise-linear behaviour formulated by Cattari and Lagomarsino (2013a). The latter in fact allows a more refined description than the bilinear formulations usually proposed by Codes (NTC18 (2018), Eurocode 8 (CEN (2005)). According to this constitutive law, the nonlinear response of masonry panels is described until very severe Damage Levels (DLs, from 1 to 5) through progressive strength degradation in correspondence of assigned values of drift. These drift thresholds are differentiated in input in the case of the pure flexural and shear failure modes; then they are properly combined also to capture hybrid modes (see Cattari and Lagomarsino (2013a) and Angiolilli et al. 2021b for further details). See Figure 1 for a sketch of the adopted constitutive law and the reference values adopted in this work. Some numerical validations of this modelling approach and software are illustrated in (Cattari et al. (2014), Marino et al (2019a), Brunelli et al. (2021), Degli Abbati et al. (2021)) by means of the comparison with experimental tests on shaking table or with the actual response of URM buildings which experienced seismic events. A concise description of this EF modelling approach is also collected in Cattari et al. (2021b), where the interested reader is referred to.

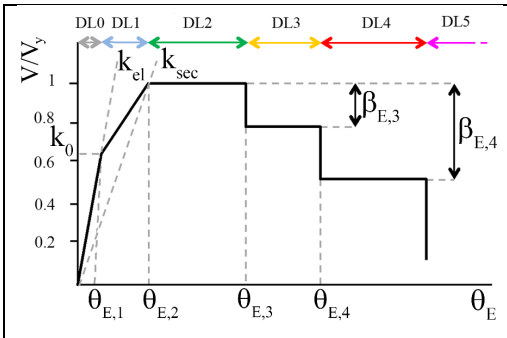

a)

	Piers [%]				Spandrels [%]			
	SHEAR		FLEXURAL		SHEAR		FLEXURAL	
	$\theta_{E,i}$	$\beta_{E,I}$	$\theta_{E,i}$	$\beta_{E,i}$	$\theta_{E,i}$	$\beta_{E,i}$	$\theta_{E,i}$	$\beta_{E,i}$
DL3	0.3	0.7	0.6	1.0	0.3	0.5	0.3	1.0
DL4	0.5	0.4	1.0	0.85	0.6	0.5	0.6	0.5
DL5	0.7	0.0	1.5	0.0	2	0.0	2	0.0

$\theta_{E,i}$: drift threshold that defines the attainment of the ith DL;
$\beta_{E,i}$: residual strength with respect to the maximum shear strength in correspondence of the ith DL

b)

Figure 1 - Sketch of the piecewise-linear constitutive law adopted (a) and parameters describing the post-peak behaviour assumed for masonry piers and spandrels (b).

2.1.2. Continuum FE model

The concrete damaged plasticity (CDP) model (Lubliner et al (1989)) is adopted in the continuum FE model. This isotropic model uses concepts of damaged elasticity together with tensile and compressive plasticity (see also Figure 3). Although originally developed to describe the nonlinear behaviour of isotropic quasi-brittle materials e.g. concrete, the CDP model has been widely adopted for the analysis of masonry structures (Milani and Valente (2015), Valente and Milani (2016), Casolo et al (2016), Milani et al (2017), Degli Abbati et al (2018), Castellazzi et al (2018)), which may show anisotropic behaviours. Indeed, despite the advancements in damage models with anisotropic response carried out for masonry (Berto et al. 2002, Pelà et al. 2013, Pantò et al. 2022), their applicability is still circumscribed in engineering practice due to the many mechanical properties needed to define the material which are not generally available. In addition, the isotropic nonlinear continuum herein used has been comprehensively tested for masonry and compared with other modelling strategies in D'Altri et al (2021). In particular, it appeared capable to catch both flexural and shear pier failures, i.e. the ones which mainly rule the behavior of horizontally loaded masonry structures. Additionally, the outcomes of this continuum model appeared promisingly comparable with other more detailed block-based models at the scale of masonry piers, in terms of both load-displacement curves and crack patterns (D'Altri et al 2021). Moreover, the effectiveness of this nonlinear continuum was already proven in Cattari et al (2021b) by analyzing the response of piers characterized by various width-to-height slenderness ratio and compressive stress states. Therefore, despite the isotropic hypothesis, this continuum model appears to be able to simulate the mechanical response of masonry piers when appropriate mechanical parameters are adopted. Higher approximations could be expected on the mechanical response of masonry spandrels, in particular when not coupled to other tensile resistant elements, that however is not the main focus of this work.

2.2. Walls configurations and numerical models

The irregular wall configurations have been defined starting from the geometry of a regular wall already analysed in Cattari et al. (2021b). In particular, starting from the geometry of the so-called "Door Wall"

tested under quasi static loading by Calvi and Magenes (1994), different types of irregularities in the opening layout have been introduced, see Figure 2. According to Parisi and Augenti (2013), the types of irregularity can be summarized as follows: i) *offset irregularity* in the vertical direction (i.e. horizontally misaligned openings), indicated with letter C; ii) *horizontal irregularity*, indicated with letter B; iii) *vertical irregularity*, indicated with letter D. In such way, the name of each configuration reflects the types of irregularity that characterize it. In particular, the configurations of type "B" (B1, BC, B2) aim to investigate the identification of the pier geometry in presence of openings with different heights at the same storey (horizontal irregularity), while the configuration BD is oriented to address the issue associated to the presence of small openings. This latter case aims to investigate the effect of the presence of very small openings, i.e. to understand whenever neglect them in EF models. Indeed, cracks orientation often seems to ignore the presence of the very small openings as suggested by the observation of masonry buildings damaged by past earthquakes.

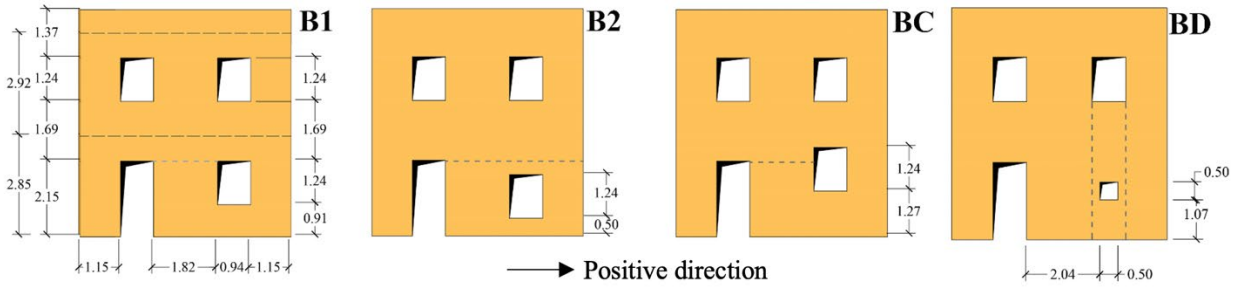

Figure 2 - Geometry of the irregular wall configurations (measures in meters).

According to the adopted methodology, a FE model (reference) and several EF models have been defined for each configuration. The various EF models are characterized by different geometries for the structural elements, as discussed in detail in Section 2.3.

The FE models of the irregular walls were defined by using 8-node linear brick elements with an approximate size of 10x10x12.5 cm (see Figure 3), in agreement with Cattari et al. (2021b). The mechanical parameters used to characterize the continuum model are the same of those adopted in Cattari et al. (2021b), i.e. Young's modulus equal to 1800 MPa, compressive strength equal to 6.2 MPa, and tensile strength equal to 0.22 MPa. For further details about the adopted mechanical properties, the

interested reader is referred to Cattari et al. (2021b). Particularly, such mechanical parameters come from a specific cross-calibration process performed in Cattari et al. (2021b) through panel-scale analyses with the aim of guaranteeing a consistent comparison between the two modelling strategies. In the calibration process the match in the initial stiffness, maximum strength and softening phase has been considered. The optimal match has been guaranteed by performing parametrical analyses varying the parameters marked in red in Figure 3a/b, that intervene in the uniaxial stress-strain relationships of the adopted constitutive law. The issue has been also recently discussed in D'Altri et al. (2021) in a more extensive way considering five different models working according to FE and discrete element approach.

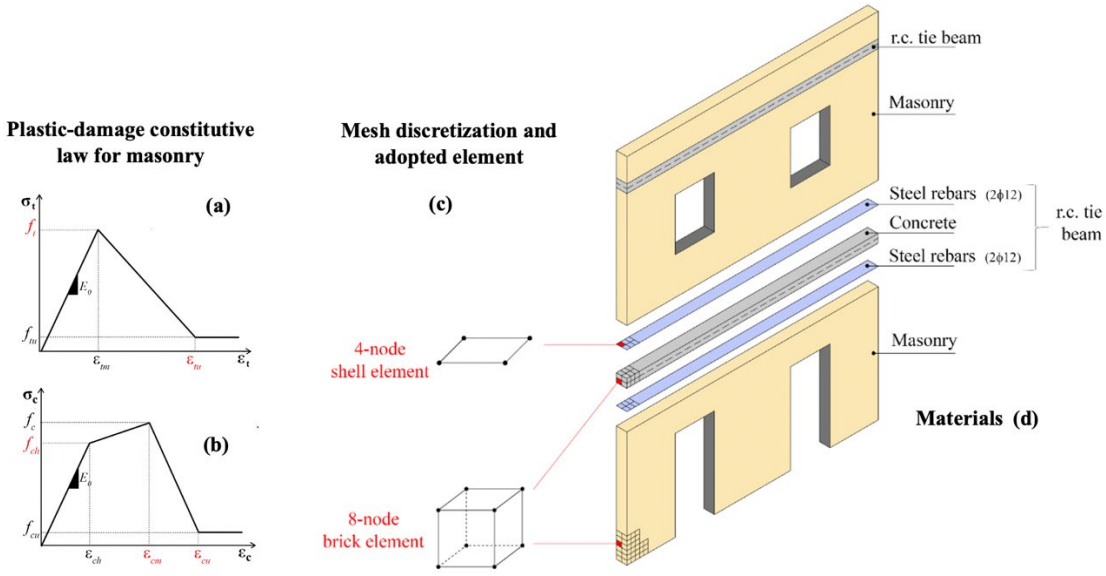

Figure 3 – Tensile (a) and compressive (b) uniaxial stress-strain relationships of the adopted constitutive law. Sketch of the mesh discretization (c) and material (d) adopted for the continuum FE model.

Figure 4 presents a summary of the outcomes of such a calibration comparing the response simulated for a panel characterised by a width-to-height slenderness ratio equal to 1.35 and for different values of the applied axial load (expressed in terms of ratio σ/fc where σ is the acting vertical stress).

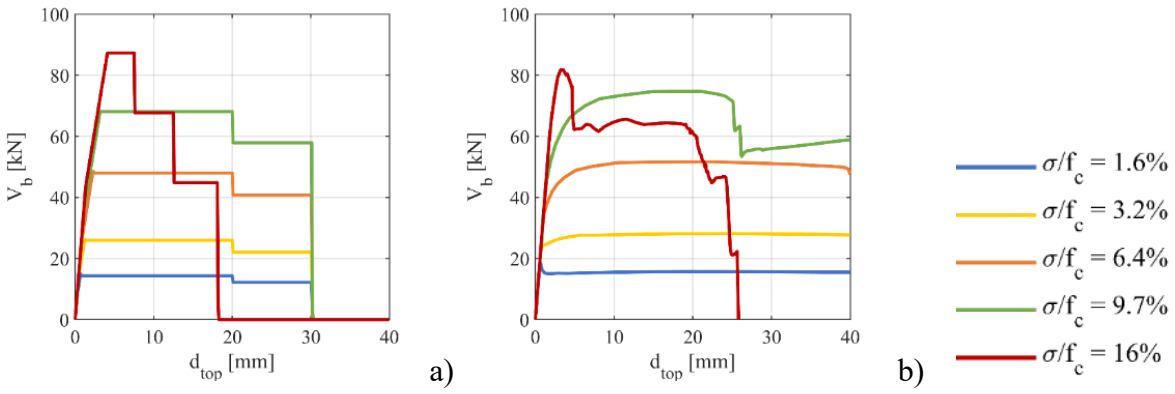

Figure 4 – Base shear-top displacement curves obtained on a single panel for different values of the applied axial load with the EF model, based on the multilinear constitutive law implemented in Tremuri program, (a) and with the FE model, based on the isotropic plastic-damaging 3D model implemented in Abaqus (b). (adapted from Cattari et al. 2021a and 2021b)

The target mechanical properties for the masonry are the same of the ones considered in Cattari et al. (2021b) and are collected in Table 1.

Table 1 – Masonry and r.c. tie beams target mechanical properties.

Parameter	**Symbol**	**Value**
Masonry Young's modulus	E_m	1800 Mpa
Masonry shear modulus	Gm	750 Mpa
Masonry compressive strength[1]	f_c	6.2 Mpa
Masonry shear strength[2]	τ_0	0.147 Mpa
Masonry specific weight	w	17.5 kN/m^3
Concrete Young's modulus	E_c	28600 Mpa
Concrete Poisson's ratio	ν_c	0.2
Concrete compressive strength	f_{cc}	24 Mpa
Concrete tensile strength	f_{tc}	1.87 Mpa
Steel Young's modulus	E_s	210000 Mpa
Steel Poisson's ratio	ν_s	0.2
Steel yield strength[3]	f_s	450 MPa

Notes:

[1] the compressive strength, in the EF model, is used to compute the strength associated with the flexural failure mode, evaluated according to CEN (2005) (i.e.by neglecting the tensile strength of the material and assuming a stress block normal distribution at the compressed toe)

2 the masonry shear strength, in the EF model, is used to compute the strength associated to the diagonal cracking failure mode, calculated according to Turnšek and Sheppard (1980)

[3] the steel yield strength, together with the area of longitudinal reinforcement present in the r.c. beam, is the parameter necessary to compute the value of H_p, consisting in the maximum axial force assumed to be developed in the spandrel. More specifically, H_p is computed as the minimum between $A_s f_s$ and $0.4 h_{sp} t_{sp} f_{ch}$, being A_s the total longitudinal reinforcement present in the r.c. beam, f_{ch} the compressive strength of masonry in horizontal direction (assumed herein equal to $0.5 f_c$), h_{sp} and t_{sp} the height and thickness of the spandrel. The value of HP in then adopted to compute the maximum strength associated to the flexural failure mode according to NTC18 (2018).

In particular, the maximum strength is computed as the minimum between the strength associated with the flexural failure mode and that associated to the diagonal cracking failure mode according to the simplified criteria proposed in literature (Calderini et al. 2009) and commonly adopted in Codes (NTC18 (2018), Eurocode 8 (CEN (2005), NZSEE (2017)). As reviewed in Beyer (2012) and Beyer and Mangalathu (2013), the behavior of spandrels in terms of maximum strength and post-peak softening phase is significantly affected by the interaction with the lintel and the potential interaction with other tensile resistant element coupled at floor level (e.g. steel tie-rods, r.c. beams). More specifically, when the latter are present, as in this case, the development of a diagonal strut is assumed likely to be activated in the spandrel. This modelling strategy, that is explicitly proposed in NTC18 (2018) (on which the strength criterion herein adopted is based), finds confirmation also in the results of several experimental campaigns (Beyer and Dazio (2012), Parisi et al (2014)). The parameters of the piecewise-linear definition of the post-peak response of both piers and spandrels, whose results are illustrated in Figure 4, are collected in Figure 1.

Four existing criteria for the identification of the structural elements (Augenti (2006), Dolce (1991), Moon et al (2006) and Lagomarsino et al (2013)) have been selected among those commonly used in engineering applications. Particularly, the empirical criterion proposed in Lagomarsino et al (2013) has been considered for the identification of spandrels. The adopted rules are empirical or based on limited experimentations and\or few numerical simulations. A review on the basics which they are based on has been recently reported in Cattari et al. (2021a). The four possible EF idealizations obtained for each wall configuration are illustrated in Figure 5. According to Moon et al. (2006) and Augenti (2006), the pier geometry changes with the loading orientation. This leads to the adoption of two different EF models in the positive and negative directions.

Figure 6 clarifies, by way of example for the B1 configuration, also the numbering adopted in the following sections for the discussion of results. Moreover, Figure 6 also specifies for the same configurations the different values of effective height (h_{eff}) and width-to-height slenderness ratio (λ) of piers varying the criterion adopted.

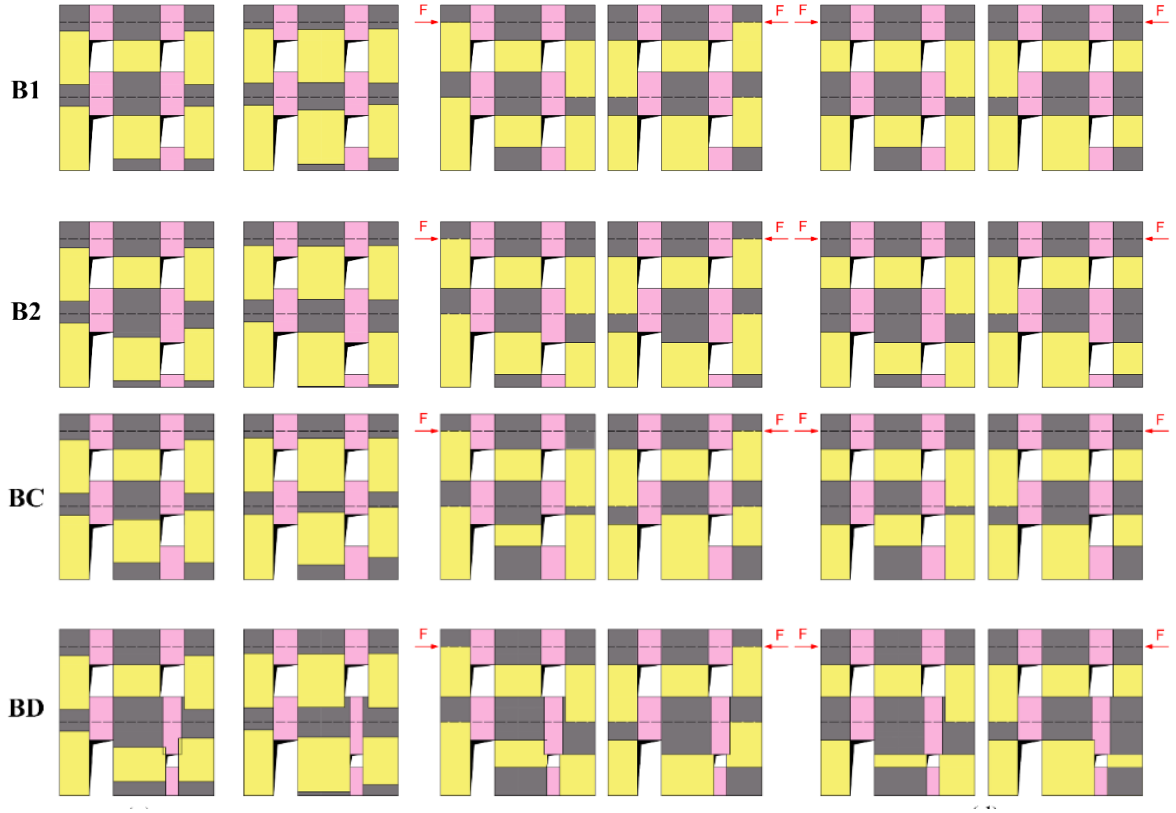

Figure 5 – EF models obtained for the introduced wall configurations; pier effective height according to: a) (a) Dolce (1991) (b) Lagomarsino et al. (2013); c) Moon et al. (2006); d) Augenti (2006). See Figure 6 for the legend of colours.

(a)

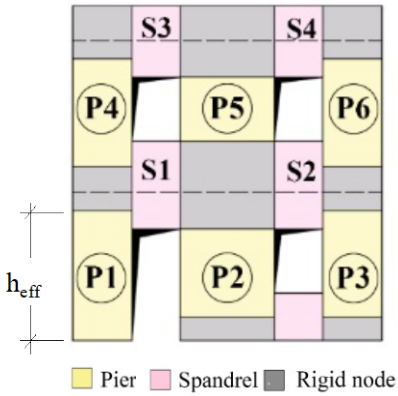

(b)

B1			(a) Lagomarsino et al. (2013)	(b) Dolce (1991)	(c) Moon et al (2006)		(d) Augenti (2006)	
					Pos	Neg	Pos	Neg
1st storey	P1	h_{eff} [m]	2.50	2.54	2.85	2.15	2.15	2.15
		λ [-]	2.17	2.20	2.48	1.87	1.87	1.87
	P2	h_{eff} [m]	1.69	2.11	1.24	2.15	1.24	2.15
		λ [-]	0.93	1.16	0.68	1.18	0.68	1.18
	P3	h_{eff} [m]	2.04	2.09	2.15	1.94	2.15	1.24
		λ [-]	1.78	1.82	1.87	1.69	1.87	1.07
2nd storey	P4	h_{eff} [m]	2.08	2.11	1.94	2.22	1.24	2.22
		λ [-]	1.81	1.83	1.68	1.93	1.07	1.93
	P5	h_{eff} [m]	1.24	2.06	1.24	1.24	1.24	1.24
		λ [-]	0.68	1.13	0.68	0.68	0.68	0.68
	P6	h_{eff} [m]	2.08	2.11	2.22	1.94	2.22	1.24
		λ [-]	1.81	1.83	1.93	1.68	1.93	1.07

Figure 6– Equivalent frame idealization of B1 configuration: a) identification and numbering of piers and spandrels; b) resulting effective height (h_{eff}) and slenderness ratio (λ) of piers varying the rule adopted.

In case of type "B" walls (see as for example configuration B1 and BC, Figure 5), the presence of the horizontal irregularity at the ground floor causes significant differences in the resulting effective height for piers across the considered criteria. These discrepancies are even clearer when moving to configuration BD, especially in the case of pier P2 (according to the numbering introduced in Figure 6),

for which very different values of λ (from a minimum of 0.25 to a maximum of 1.05) are associated to. On the basis of the results on regular walls obtained in Cattari et al. (2021b), the effective length of the r.c. tie beams is assumed in the EF models equal to the net width of the corresponding opening.

Nonlinear static analyses have been performed by adopting a uniform load pattern and by considering both positive and negative directions. In the FE model, displacement-control analyses have been conducted through the introduction of a rigid beam with the end sections located at the level of the diaphragms, linked to the nodes of the wall mesh to obtain an isostatic system. Then, the horizontal displacement of a control node located on it has been progressively increased.

The loads at the lower and upper floors have been assumed to be 20.7 and 19.7 kN/m, respectively. These values are compatible with those associated to common r.c. diaphragms (in agreement with the assumption of r.c. beams coupled to spandrels at floor level).

2.3. Equivalent Frame and Finite Element comparison criteria

The comparison between EF and FE modelling strategies involves different aspects of the structural response, particularly in terms of (i) global response; (ii) damage pattern, and (iii) local response (generalized forces and displacements). The global response comparison consists of the comparison of pushover curves and other global response parameters (GRPs). Particularly, GRPs aim to evaluate the scatter from the reference solution, typically in terms of global stiffness, maximum strength, and post-peak response. In this paper, the same four GRPs utilized in Cattari et al. (2021b) are considered. In particular, they are: (i) the secant stiffness $k_{s,35}$ linked to the 35% of the maximum global strength, (ii) the rate $R_k = k_{s,70}/k_{s,35,}$ being $k_{s,70}$ the secant stiffness linked to the 70% of the maximum global strength, (iii) the maximum value of global strength V_{max}, and (iv) the top displacement $d_{top,n}$ linked to a strength reduction of 30% and 15%, i.e. $d_{top,15}$ and $d_{top,30}$. More details on how the scatter in the GRPs (i.e. ΔGRP) has been computed can be found in Cattari et al. (2021b) and it has been shortly recalled in Figure 9.

Regarding the generalized forces and displacements (ii) comparison, specific horizontal and vertical alignments have to be specified for their computation. Some examples are illustrated in Figure 7, where bold red lines indicate the position of the reference point that was considered in the corresponding cross sections for the computation of the bending moment.

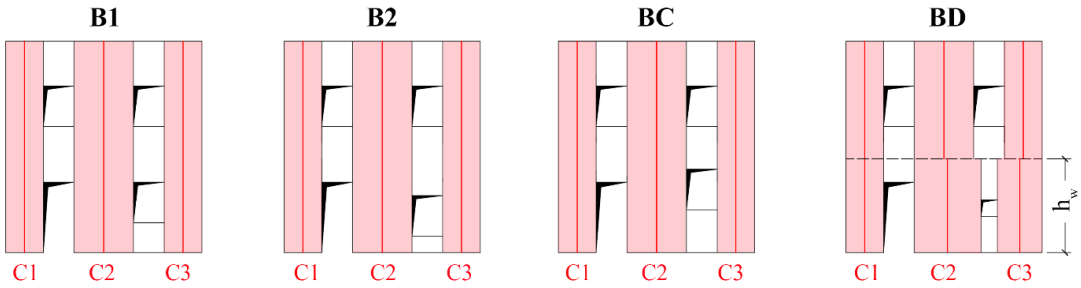

Figure 7 – Vertical alignments (C1, C2 and C3) considered in the configurations (h_w = interstorey height).

3. IDENTIFICATION OF THE PIER EFFECTIVE HEIGHT IN CASE OF HORIZONTAL IRREGULARITY

3.1. Results on B1, B2 and BC configurations: global response

In Figure 8, the comparison among the pushover curves obtained with the different numerical models is presented in case of configuration B1, for both positive and negative directions of the analysis.

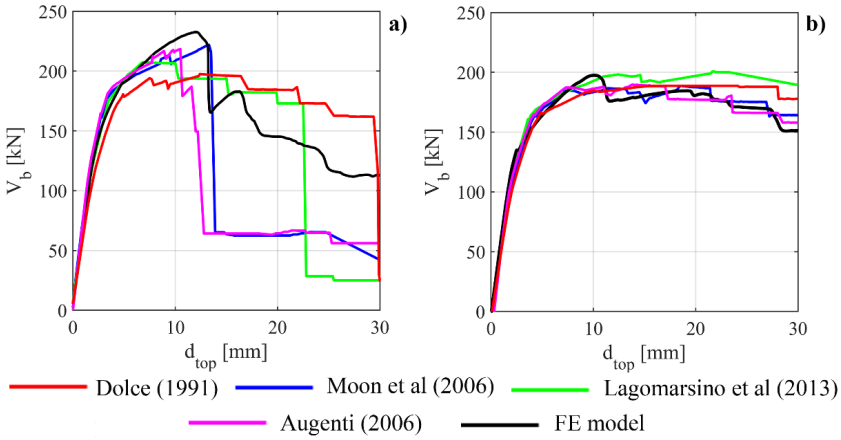

Figure 8 - Comparison in terms of pushover curves for configuration B1: a) analysis in the positive direction; b) analysis in the negative direction.

In the negative direction (Figure 8b), the different EF models provide quite similar results in terms of global response, with only slight discrepancies in terms of stiffness and maximum strength. Moreover, these results are close to the reference solution provided by the FE model (black curve). More significant differences can be instead detected in the positive direction (Figure 8a); in fact, the scatter of the results provided by the EF models remarkable, especially in the post-peak phase.

This difference can be explained by considering that, in the positive direction, the part of the wall that gives the higher contribution to the structural response (i.e. the part where the compression stresses increase) is the one where the irregularity is present. Indeed, here the criteria for the pier effective height

give different recommendations (see previous Figure 5). Particularly, it may be noted that the models consistent with Moon et al (2006) and by Augenti (2006) provide a good description of the behaviour only until the maximum strength while then they predict a sudden drop of strength in correspondence of a top displacement approximatively equal to 13 mm. However, the strength degradation in the curve of the FE model is more gradual and tends to be more in agreement with the one described by the models based on Dolce (1991) and Lagomarsino et al (2013). Very similar considerations can be made also for configurations B2 and BC, for which, for sake of brevity, the complete results in terms of pushover curves are omitted.

These observations are confirmed by the results in terms of scatter on the GRPs with respect to the FE model (Figure 9). Concerning $k_{s,35}$, for all the configurations, it is possible to observe that the adoption of the criterion suggested by Dolce (1991) leads to the lowest scatter with respect to the FE model (i.e. $\Delta k_{s,35}$ almost equal to 0). Moreover, also the proposal by Lagomarsino et al (2013) allows to obtain good results, with an overestimation of the initial stiffness which is in general lower than 15%. On the contrary, the criteria proposed by Moon et al (2006) and by Augenti (2006) produce values of $\Delta k_{s,35}$ considerably higher, with values in some cases close to 50% (see e.g. configuration BC). According to these rules in fact rather squat piers are introduced in the model. The scatter with respect to the parameter R_k is lower than 10% in almost all the cases, thus indicating the capability of the EF models to well capture the stiffness degradation phenomenon occurring in the FE model. In this case, no significant difference among models set with the different rules is detected.

Similar considerations can be made in terms of maximum strength. The values of ΔV_{max} are in almost all the cases lower than 10%. In general, EF models tend to underestimate the maximum strength with respect to the FE model ($\Delta V_{max} < 0$). However, it is worth pointing out that the seismic safety verification based on nonlinear static analyses usually requires the conversion of the pushover curve into an equivalent bilinear (Marino et al. 2019b). This latter is expected to further smooth these differences.

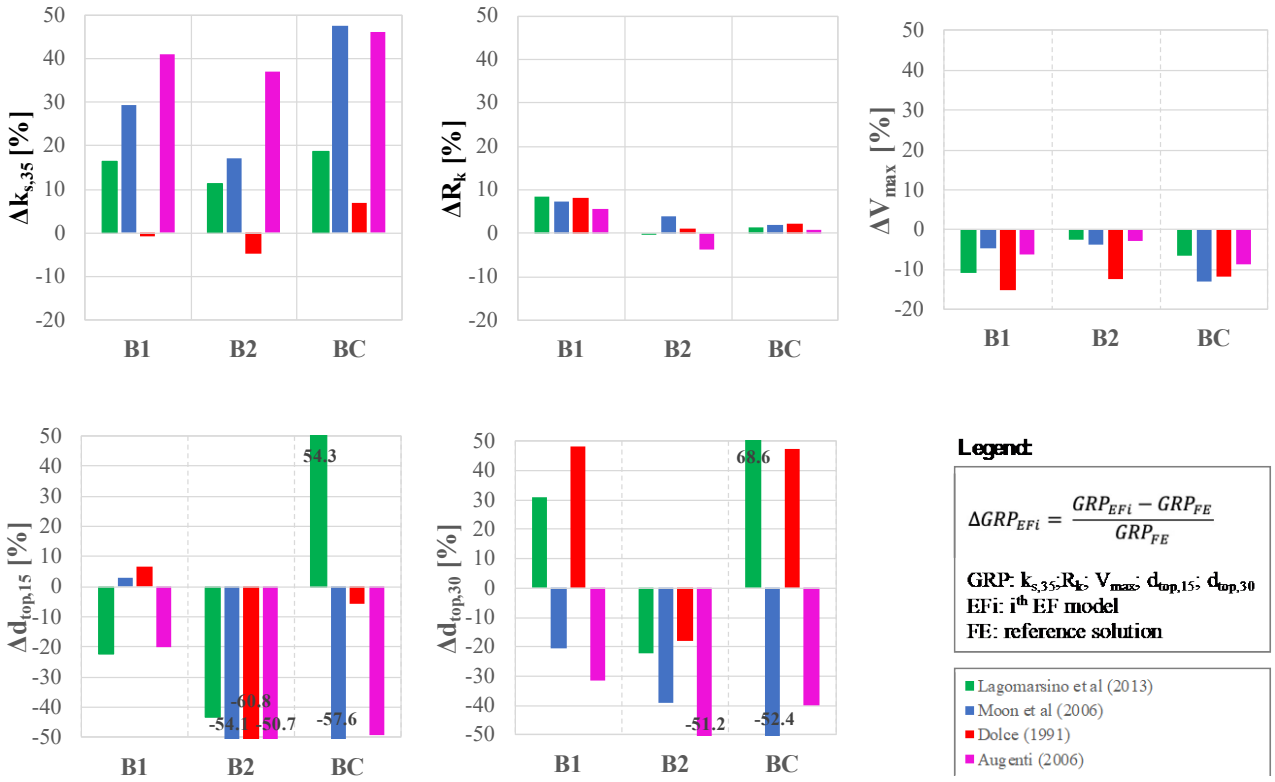

Figure 9 – Comparison of the results in terms of ΔGRP (scatter of the Global Response Parameters with respect to the FE model) obtained through the EF models defined according to the different criteria for the EF idealization and for configurations B1, B2 and BC; positive direction of the analysis.

The results in terms of $d_{top,15}$ and $d_{top,30}$ substantially confirm what seen in the global pushover curves. Indeed, a high scatter with respect to the FE model can be observed. The results referring to configuration B1 help to quantify the considerations previously made on the comparison between the pushover curves in terms of post-peak phase. As a confirmation of that, also in case of configuration BC, the criteria proposed by Moon et al (2006) and by Augenti (2006) lead to a high underestimation of the displacement capacity with respect to the FE model (scatter on $\Delta d_{top,15}$ and $\Delta d_{top,30}$ in general higher than 50%); that is related to the premature drop of strength observed in the pushover curves associated to these models. Also, the EF model based on Lagomarsino et al (2013) shows a significant scatter on $\Delta d_{top,15}$ and $\Delta d_{top,30}$, which in this case is due to an opposite situation (i.e. underestimation of the strength degradation with respect to the FE model). On the contrary, the criterion proposed by Dolce (1991) provides in general better results, especially when considering $d_{top,15}$.

Moving to configuration B2, similar observations apply to the cases based on Moon et al (2006) and by Augenti (2006). Conversely, the criterion suggested by Lagomarsino et al (2013) leads to a scatter with

respect to the FE model lower than the other criteria when considering both $d_{top,15}$ and $d_{top,30}$, while Dolce's rule works well when considering a high level of strength degradation ($\Delta d_{top,30}$ within 15%).

3.2. Results on B1, B2 and BC configurations: damage pattern

In Figure 10, the comparison between the damage pattern resulting from the FE model and from two EF models (Augenti (2006) and Dolce (1991)) is illustrated, by way of example in the case of configuration B1 (positive analysis). In particular, damage refers to three increasing values of the top displacement. Similar results are obtained also in the case of configurations BC and B2.

The attention is focused on the element P2 (see the numbering of Figure 6), which basically governs the global response predicted by the EF models (carrying almost 60% of the total base shear) and is characterized by highest differences in the geometry across the four considered rules. At a top displacement equal to 15 mm, the EF model based on Augenti (2006) predicts the actual collapse (DL5) for P2, i.e. the total loss of strength (see also Figure 1 for the physical meaning associated to the progressing damage levels). The same is also observed for the model based on Moon et al (2006). Conversely, according to the EF model defined on the basis of Dolce's criterion, P2 pier is characterized by a lower state of damage (DL2), substantially corresponding to the attainment of the maximum strength but still exhibiting some residual strength with respect to the horizontal actions. The model according to Lagomarsino et al (2013) produces similar results. This explains the different strength degradation observed in the pushover curves associated to the different EF models.

It should be stressed that the failure of masonry panels is governed by the reaching of fixed values of drift in EF models. Consequently, the failure of rather squat panels for very low values of the horizontal displacement affects the global ductility of the system. Moreover, under the same hypotheses and boundary conditions, when the aspect ratio of a panel reduces, a shear failure is more likely to occur than a flexural failure, and the shear failure is associated to lower values of drift thresholds with respect to flexural one, being characterized by a more fragile response. This is exactly what happens in case of the EF models according to the criteria proposed by Moon et al (2006) and by Augenti (2006), where the geometry characterizing P2 is particularly squat ($\lambda = 0.67$). Conversely, in the other EF models

(Dolce (1991) and Lagomarsino et al (2013)), where P2 is not so squat (having $\lambda = 1.16$ and $\lambda = 0.93$, respectively), the sudden drop of strength observed in the other two models does not occur.

By comparing the damage pattern obtained in the FE model with those predicted by the four EF models (Figure 10), a quite good agreement is in general observed. In fact, all models agree in predicting a flexural failure for the piers at the upper storey and a concentration of a more significant damage in the pier panels at the ground floor. In particular, all the EF models predict a flexural failure for P1, which is consistent with what emerges also from the FE model.

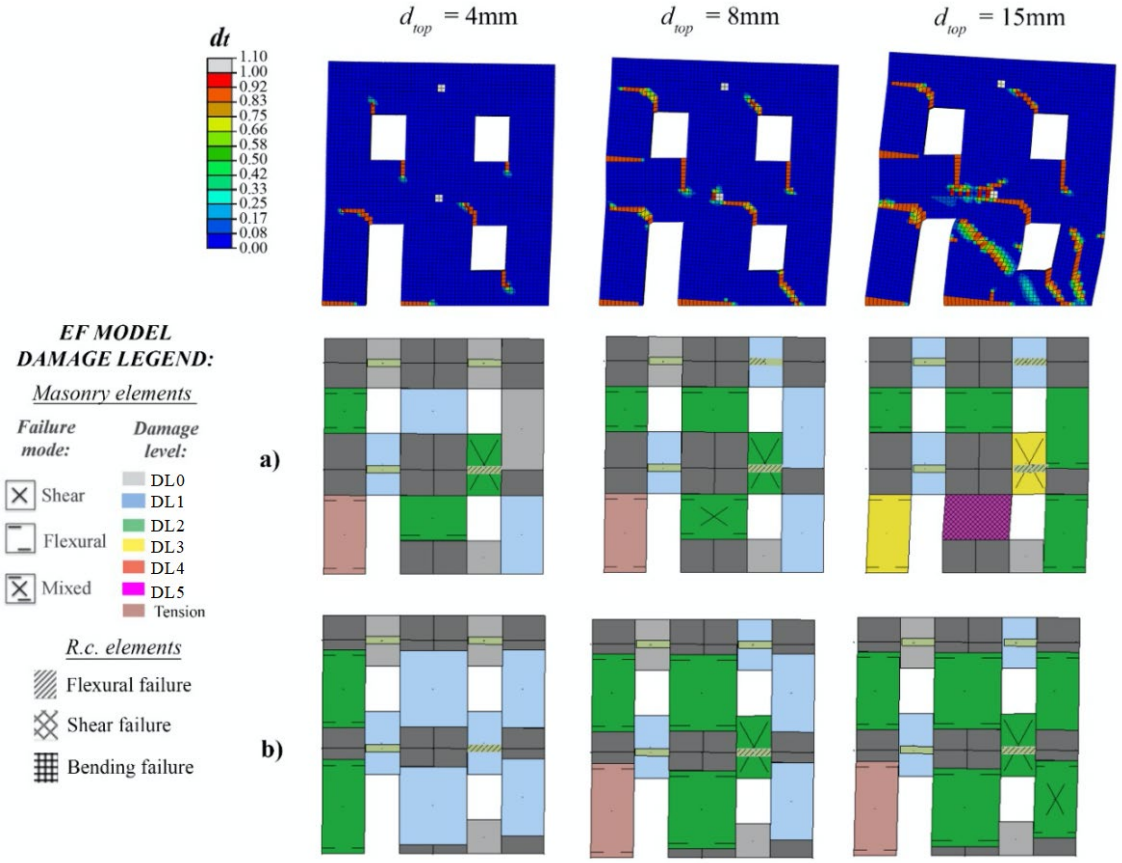

Figure 10 - Configuration B1, analysis in the positive direction: comparison between the damage pattern resulting from the FE model and the EF models associated to the different criteria for the pier effective height: a) Augenti (2006); b) Dolce (1991)

When considering P2 and P3, more differences arise. Indeed, the EF model based on Dolce (1991) predicts for the element P3 a hybrid failure, as in the FE model, while the application of the Augenti's criterion leads to a flexural failure. For the element P2, the EF model based on Augenti (2006) predicts a hybrid failure, which is consistent with the tensile cracks observed in the FE model in the corresponding portion of masonry, interested by the propagation of a diagonal crack but also by the

parzialization of the end sections. Conversely, the other EF models show a prevailing flexural failure for P2, being characterized by a higher aspect ratio. This can explain the higher displacement capacity characterizing the structural response in this case, and also why the maximum global strength predicted by the model according to Dolce (1991) is slightly lower than the one obtained with the other model here considered (see the pushover curves in Figure 8). The model based on Moon et al (2006) leads to results similar to the model based on Augenti (2006), while the one defined on the basis of Lagomarsino et al (2013) provides results closer to those obtained through Dolce (1991).

Considering the analyses in the negative direction, no significant differences are detected in the damage pattern predicted by the four EF models. Moreover, the evolution of damage and the types of failure occurring in the panels are substantially consistent with the predictions of the FE model. This is coherent with the global responses provided by the considered numerical models (Figure 8b).

3.3. Results on B1, B2 and BC configurations: local response

Moving to the analysis of the local response, in Figure 11 three base sections were considered for the computation of the reaction forces (i.e. the normal force, shear force and bending moment).

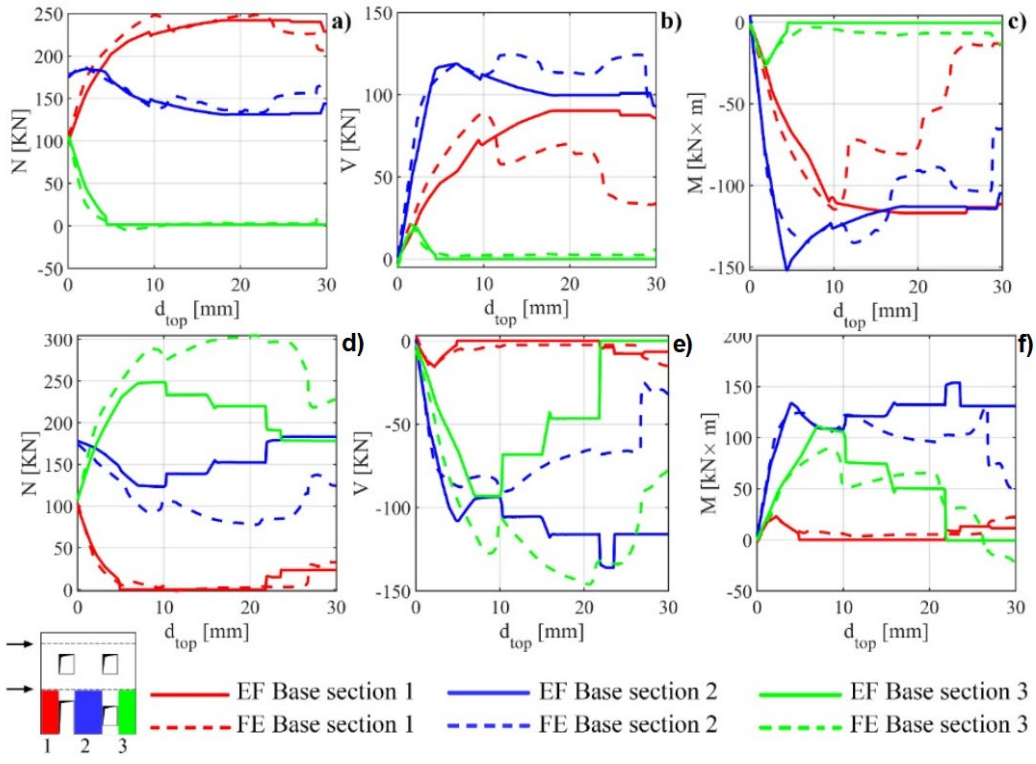

Figure 11 – Configuration B2: comparison on generalized forces at the base sections of the wall between the FE model and the EF model based on Dolce (1991): normal force (a/d); shear force(b/e); bending moment (c/f). a/b/c: negative analysis; d/e/f positive analysis

By way of example, results refer to configuration B2 and the EF model set according to the Dolce's criterion. When considering the analyses in the negative direction (Figure 11a/b/c), the comparisons of the evolution of the reaction forces show that a good agreement. This result is substantially confirmed by all EF models. On the contrary, when considering the results of the analyses in the positive direction (Figure 11d/e/f), a quite good agreement with the FE model can be observed in the initial phase of the response, while more differences arise when the structural response becomes strongly nonlinear.

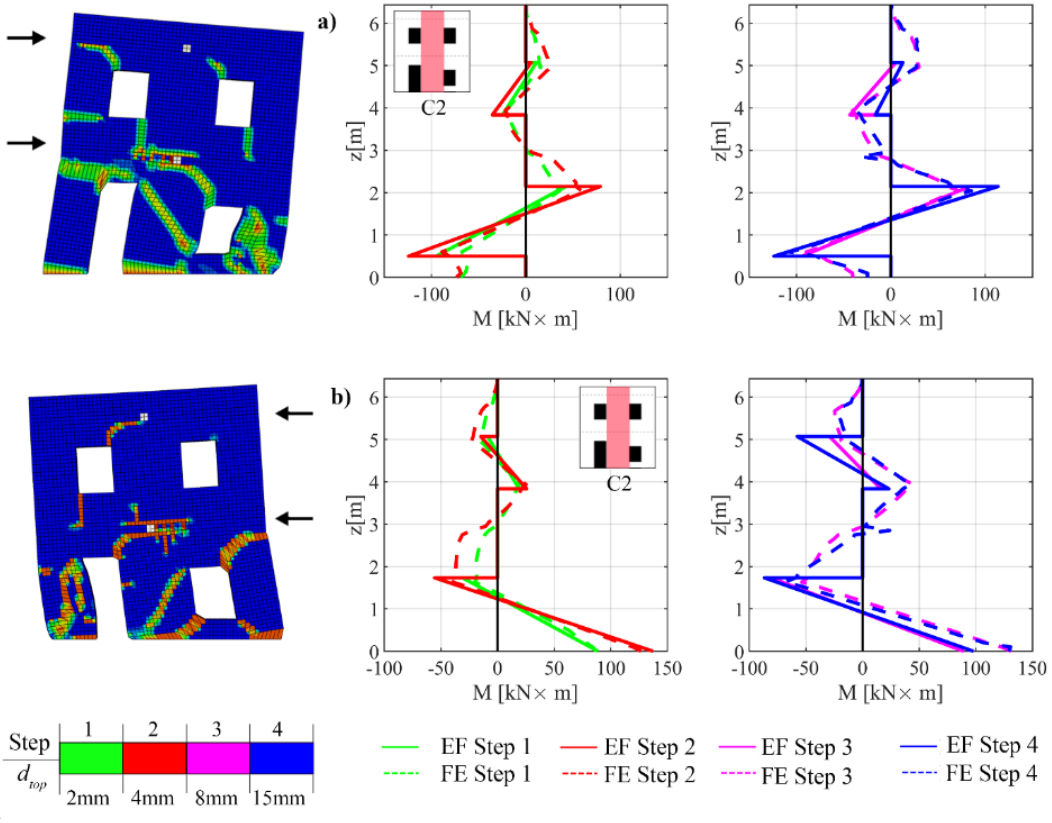

Figure 12 – Configuration B2, analysis in the positive direction (a) and in the negative direction (b): on the left tensile damage deriving from the FE analysis (d_{top} = 30 mm) and on the right comparison between the FE model and the EF models according to Moon et al (2006) in terms of bending moment *M* acting on the vertical alignment C2.

Concerning the comparison in terms of generalized forces, the results associated to the alignment C2 (see Figure 7) are of particular interest, as C2 includes at the ground floor the pier P2. They are firstly reported in Figure 12 for configuration B2 and adopting the EF model according to Moon et al. (2006). More specifically, a comparison of bending moment diagrams at different steps of the analysis between the FE model and the EF model based on Moon et al (2006) is given in Figure 12; in addition, the damage pattern experienced in the FE model (d_{top} = 30 mm) is also illustrated. The latter is useful to

identify the portions of masonry where damage is concentrated; in other words, it may help the identification of the piers effective height. Indeed, it is possible to observe that the propagation of the tensile cracks in the FE model actually changes depending on the direction of the analysis and is consistent with the rule of the compression strut, on which the proposal by Moon et al (2006) is based. Also, the analysis of the local response in terms of bending moment diagram shown in Figure 11 confirms that the effective height predicted for pier elements by this criterion is in good agreement with the FE model. This result was confirmed also in case of configurations BC and B1.

Figure 13 shows the comparison of the results on alignment C2 for the configuration BC and for the EF models based on Moon et al (2006), Lagomarsino et al (2013) and Dolce (1991).

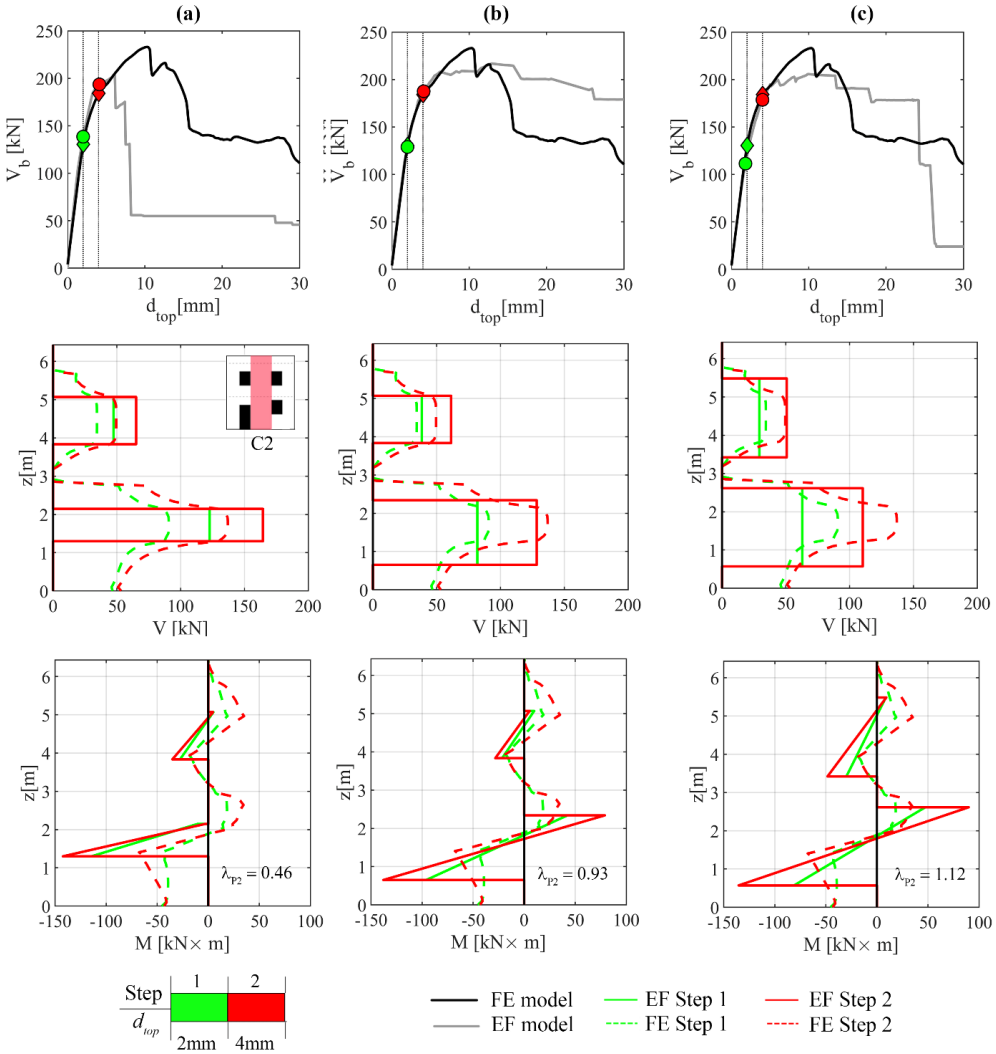

Figure 13 - Configuration BC, analysis in the positive direction: comparison between the FE model and different EF models ((a) Moon et al (2006), (b) Lagomarsino et al (2013), (c) Dolce (1991)) in terms of shear force *V* and bending moment *M* acting on the vertical alignment C2 for two different steps of the analysis; λ_{P2} is the aspect-ratio of pier P2.

The results of the EF model based on Augenti are not shown, being very similar to Moon et al (2006). Also in this case, the EF model based on Moon et al (2006) is capable to well capture the effective height predicted by the FE analysis. However, the shear force diagrams in Figure 13 show that the model which provides the best match with the results of the FE model is the one based on Lagomarsino et al (2013). Indeed, the model based on Moon et al (2006) overestimates the shear force, especially in case of the pier at the ground floor. On the contrary, the model based on the Dolce's criterion tends to underestimate the shear force acting in P2. These results are related to the fact that the effective height predicted by the criterion suggested in Lagomarsino et al (2013) for the pier at the ground floor (P2) is intermediate between the ones predicted by the other two criteria. The EF model based on Lagomarsino et al (2013) actually provides a better description, with respect to the other models, also in terms of bending moment diagram.

For the configuration B1 (Figure 14), it can be seen that the EF model based on Lagomarsino et al (2013) (Figure 14b) still provides good results in terms of both shear force and bending moment, considering the piers at the two floors. It should be highlighted that in the model based on the Moon's criterion (Figure14a), the shear force and bending moment acting in P2 at step 4 are equal to zero, having this element already reached the actual collapse for the considered value of top displacement (d_{top} = 15 mm, see Figure 8). This indicates that Moon's criterion does not provide a well description of the actual local response.

Figure 15 shows the comparisons in terms of deformed shapes associated to the vertical alignment C1. Particularly, the results of the FE model are compared with the ones derived from the EF models based on Augenti (2006) and Dolce (1991). Generally, it can be noted that the EF models associated to the criteria suggested by Dolce (1991) and Lagomarsino et al (2013) provide results closer to the FE model with respect to the other two EF models.

Finally, the comparison in terms of drift values associated to the masonry piers is discussed in the following. Figure 16 shows the comparison in terms of drift in the case of positive analysis on configuration B1. The attention is here focused on the three piers at the ground floor, where the damage

is mainly concentrated. It is observed that more differences are detected on the central pier (P2) rather than the external piers (P1 and P3).

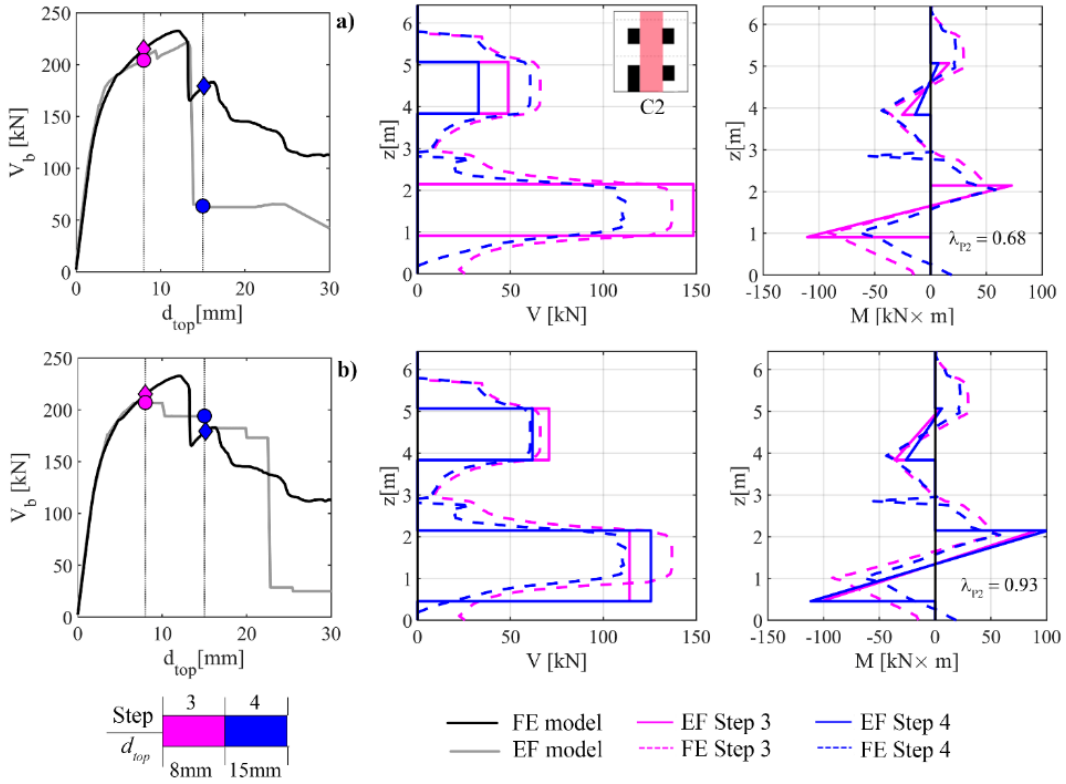

Figure 14 - Configuration B1, analysis in the positive direction: comparison between the FE model and different EF models (a) Moon et al (2006), b) Lagomarsino et al (2013)) in terms of shear force *V* and bending moment *M* acting on the vertical alignment C2 for different steps of the analysis.

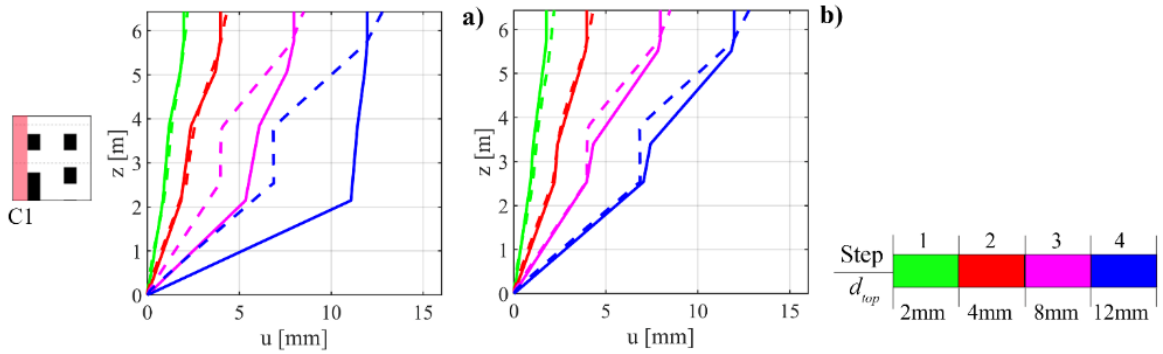

Figure 15 - Configuration BC, analysis in the positive direction: comparison between the FE model and different EF models (a) Augenti (2006) b) Dolce (1991)) in terms of deformed shapes associated to the vertical alignments C1 for different steps of the analysis.

In this case, the EF models based on Moon et al (2006) and Augenti (2006) significantly overestimate the value of drift in correspondence of step 4 with respect to the results derived from the FE model. This result indicates that the adoption of these criteria leads, in this case, to an incorrect description of the deformations occurring in the corresponding masonry portion of the wall. Indeed, the introduction of

significantly squat piers (and consequently big rigid nodes) in the model produces a high concentration of damage in a limited portion of the wall. This is rather unrealistic as in the real masonry structures no rigid nodes are present, and the deformations are distributed in bigger portions of masonry, as actually emerges from the FE analysis. Therefore, the EF models based on the other two criteria (Lagomarsino et al (2013) and Dolce (1991)), which predict for P2 a higher effective height, allow to obtain a more accurate description of the state of deformation. The different predictions in terms of drift values provided for P2 by the four EF models help to explain what previously observed in the post-peak phase of the global pushover curves and in terms of occurred damage. Similar results have been obtained also when considering the positive analyses on the other two configurations (B2 and BC).

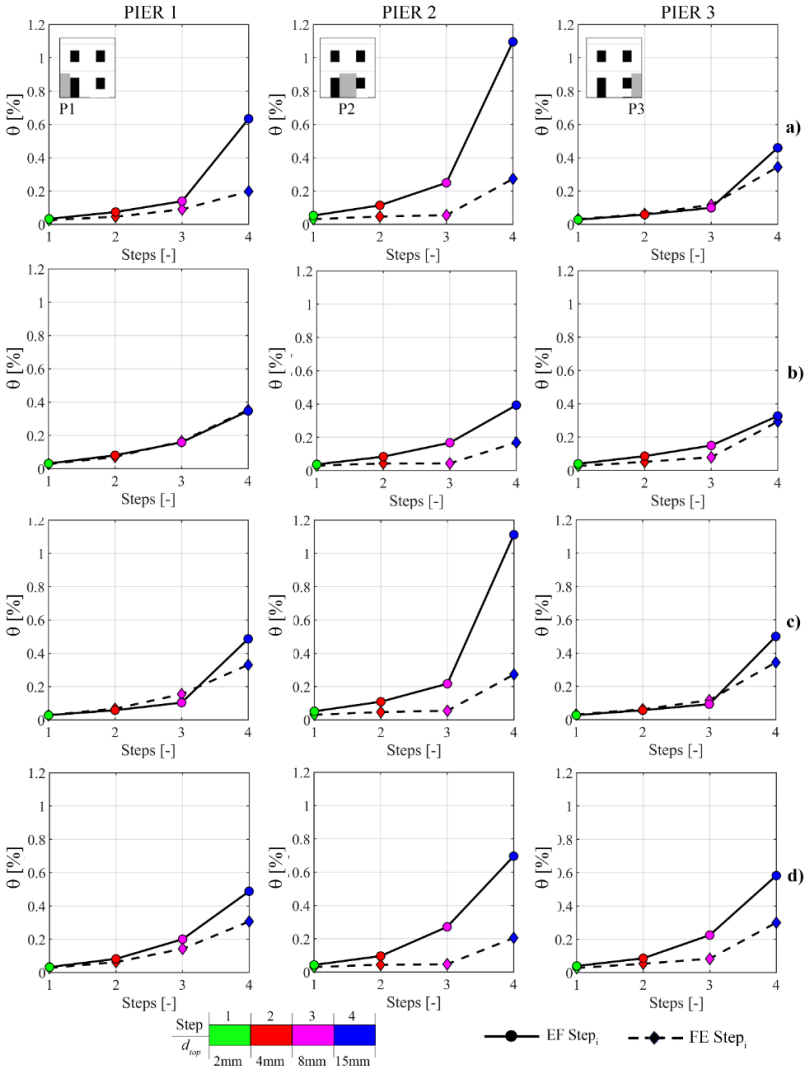

Figure 16 - Configuration B1, analysis in the positive direction: comparison in terms of drift values associated to the three piers at the ground floor between the FE model and different EF models (a) Augenti (2006); b) Dolce (1991) c) Moon et al (2006); d) Lagomarsino et al (2013)) for different steps of the analysis.

3.4. Directions from the results achieved on B1,B2 and BC configurations

The results obtained from the above discussed comparisons are further summarized in Figure 18 with the aim of expressing a more synthetic and overall effective judgment on the reliability of various examined rules. In particular, a synthetic judgment has been expressed according to the criteria introduced in Figure 17, that establishes the labels (composed by the judgment grade and an associated colour) adopted in Figure 18. In the case of the global response, the average of the absolute values of ΔGRPs (named $\mu_{\Delta GRP}$) obtained by considering all the wall configurations analysed for the examined problem (B1, B2, BC) has been computed. The GRPs assumed as reference are: $k_{s,35}$, V_{max} and $d_{top,n}$. In this last case, the average between the absolute values of $\Delta d_{top,15}$ and $\Delta d_{,top30}$ has been considered. Accordingly, for each considered GRP and each rule, a unique value of $\mu_{\Delta GRP}$ is obtained.

As far the forces and drift concern, the judgment is expressed from a qualitative point of view and based on the above discussed considerations on B1, B2, BC configurations. In attributing the judgment, particular attention has been paid to the agreement captured for pier P2, which is the element carrying almost 60% of the total base shear. As far the damage pattern concerns, the results are summarized by taking into account the capability of the model to well capture both the global failure mode (global failure) and the local damage in single pier elements (damage in piers). For the latter, particular attention has been paid to the piers at the ground floor (P1, P2, P3), where damage mainly concentrates.

A - Global response			
0 ≤ $\mu_{\Delta GRP}$ ≤ 15%	**15% < $\mu_{\Delta GRP}$ ≤ 35%**	**35% < $\mu_{\Delta GRP}$ ≤50%**	**$\mu_{\Delta GRP}$ > 50%**
LOW difference (L)	MODERATE difference (M)	HIGH difference (H)	VERY HIGH difference (VH)
B - Generalized forces, drift, damage pattern (global failure)			
Well captured	Moderate difference	Not good	
C- Damage pattern in piers			
f – Flexural failure in FE	**h** – hybrid failure in FE	**s** – shear failure in FE	
f – Flexural failure in EF	h – hybrid failure in EF	s – shear failure in EF	

Figure 17 - Criteria adopted to attribute a synthetic judgment (in terms of labels and associated colour) to the results obtained with the four EF models: global response, local response (generalized forces and drift) and damage pattern.

In all the cases, the data reported in Figure 18 refer to the most punitive between the analyses performed in the two directions (i.e. the one associated to the highest scatter of the results with respect to the FE model), that in this case is always the one in the positive direction. Indeed, the concept is that the adoption of the given criterion should produce good results for both directions, being this necessary for verification purposes.

From the overall overview provided by Figure 18, the criteria by Augenti (2006) and Moon et al (2006) are not recommended in presence of horizontal irregularity. This is due to the fact that the adoption of the criterion by Moon et al. (2006) and, even more, of the one proposed by Augenti (2006) leads to very squat piers and so large rigid nodes, thus strongly affecting also the initial stiffness of the structure. Besides that, the issue related to the relationship between height of the panel and drift estimate is relevant for the potential influence on the global ductility of the pushover curve. This is what happens in these cases, where premature drops of strength are observed, mainly due to the prevalence of shear failures. It is important to highlight that this happens despite the calibration performed at the scale of single panels between the adopted constitutive models. Therefore, this indicates a response which is not consistent with the reference solution. Moreover, the comparison in terms of local response showed a high concentration of deformation in small portions of the wall, which is rather unrealistic.

		Moon et al (2006)			Augenti (2006)			Lagomarsino et al (2013)			Dolce (1991)		
Global response	V_{max}	L			L			L			L		
	$d_{dep,n}$	H			H			M			M		
	$k_{s,35}$	H			H			L			L		
Damage pattern	**Global failure**	Well captured			Well captured			Well captured			Well captured		
	Damage in Piers	**B1**	**B2**	**BC**	**B1**	**B2**	**BC**	**B1**	**B2**	**BC**	**B1**	**B2**	**BC**
	P1	f/f	f/f	f/f	f/f	f/f	f/f	f/f	f/f	f/f	f/f	f/f	f/f
	P2	h/h	h/f	h/h	h/h	h/f	h/s	h/f	h/f	h/f	h/f	h/h	h/f
	P3	h/f	h/s	h/f	h/f	h/s	h/f	h/h	h/h	h/h	h/h	h/h	h/h
Generalized forces	**Shear force**	Not good (Overestimated)			Not good (Overestimated)			Well captured			Moderate Diff.		
	Bending moment	Not good			Not good			Well captured			Well captured		
Drift		Not good (Overestimated)			Not good (Overestimated)			Well captured			Well captured		

Figure 18 - Summary of the main outcomes obtained in case of the B configurations (B1, B2, BC)

Conversely, the criteria indicated in Lagomarsino et al (2013) and Dolce (1991) propose a higher effective height obtaining a better description of the behaviour, at both global and local responses. In particular, the application of the rule proposed by Dolce (1991) allowed to obtain the best observed

results in terms of deformed shapes in almost all the examined cases. Therefore, the obtained results support the idea that the rules for the identification of the pier effective height suggested in Lagomarsino et al (2013) and in Dolce (1991) can be applied without specific corrective measures.

4. PRESENCE OF SMALL OPENINGS

4.1. Results on BD configuration: global response

In Figure 19, the results in terms of global pushover curves are shown for configuration BD. In addition to models set with the four rules aforediscussed, a further model which neglects the presence of the small opening (named in the following "No window") has been considered. Particularly, this represents a possible modelling choice in the case of presence of small openings. In this model, the pier effective height is determined according to Lagomarsino et al (2013).

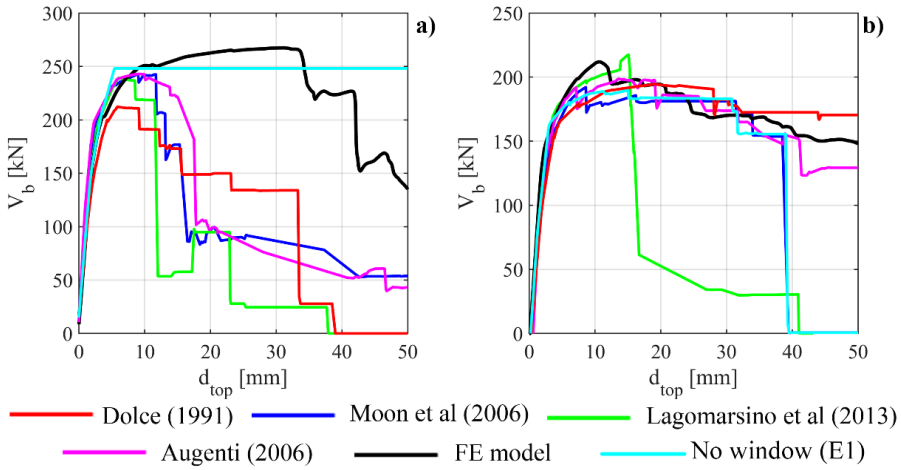

Figure 19 - Comparison in terms of pushover curves for configuration BD: a) analysis in the positive direction; b) analysis in the negative direction.

Firstly, when considering the analyses in the positive direction (Figure 19a), considerable differences can be noted in the predictions of the different EF models, both in the ascending branch of the curves and in the post-peak response. All the curves obtained with the EF models obtained by considering the presence of the small opening in applying the EF idealization rules provide global responses which are substantially different from the pushover curve associated to the FE model. On the contrary, the "No window" model provides a better match with the reference solution.

The computation of GRPs allows to better quantify these differences (see Figure 20). Indeed, it emerges that all the EF models which include the small opening, with the only exception of the one associated to

the Dolce's proposal, tend to overestimate the actual initial stiffness ($k_{s,35}$). This is particularly true for the EF model based on the Augenti's criterion, where the difference with respect to the FE model is higher than 80%. Anyway, the "No window" EF model also provides a quite good estimate of the initial stiffness, with a scatter of only 10% with respect to the FE model.

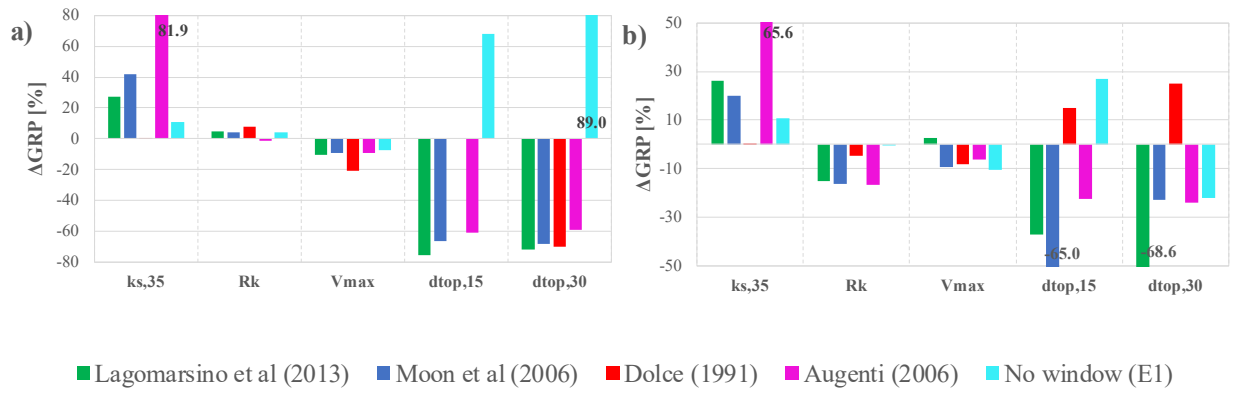

Figure 20 - Comparison of the results in terms of ΔGRP (scatter of the Global Response Parameters with respect to the FE model) obtained through the different EF models in case of configuration BD, analysis in the: (a) positive direction and (b) negative direction.

The stiffness degradation, expressed through the parameter R_k, is similar for all the considered models and it highlights a good agreement with the FE model ($\Delta R_k < 10\%$).

Concerning the maximum strength V_{max}, all the EF models slightly underestimate of about 10% the maximum strength recorded by the FE model. In the EF model based on the Dolce's criterion this underestimation is even higher, and approximatively equal to 20%. On the contrary, the "No window" EF model provides a result closer to the one of the reference solution.

The analysis of the post-peak response characterizing the pushover curves represented in Figure 19a shows that, all EF models set according to the four considered rules predict a significant strength degradation which occurs for values of top displacement ranging from 12 mm to 18 mm. This type of behaviour is considerably different with respect to the reference solution and leads to very high values of the scatter on the parameters $d_{top,15}$ and $d_{top,30}$. Indeed, all the EF models are associated to an underestimation of these parameters which is on average about 65%. In the case of the model according to Dolce (1991), since the scatter with respect to V_{max} is higher than 15%, it is not possible to compute $\Delta d_{top,15}$. On the contrary, in the curve obtained through the "No window" EF model no strength

degradation is observed for the examined values of top displacement. Accordingly, a better match with the considered reference solution, at least until a top displacement of 35 mm, is obtained. Nevertheless, this EF model does not well capture the strength decay observed in the FE model for higher values of top displacement, as evidenced by the significant values of $\Delta d_{top,15}$ and $\Delta d_{top,30}$.

In the negative direction, a better agreement between the predictions of the different EF models can be observed (Figure 19b) apart EF model based on Lagomarsino et al (2013) that exhibits a considerable strength reduction in correspondence of a top displacement equal to 16 mm. This is mainly due to the failure of the central pier at the ground floor, as better explained in section 4.2.

The scatter of the other GRPs (Figure 18b) also shows that by using the "No window" EF model is possible to obtain results which are closer to the FE solution, especially in terms of stiffness degradation (ΔR_k almost equal to zero) and initial stiffness $\Delta k_{S,35}$ (in this case is equal to 10%).

4.2. Results on BD configuration: damage pattern

In the following, the analysis of the experienced damage pattern is presented, focusing the attention on pier P2. Figure 21 shows the damage pattern for a top displacement equal to 15 mm, considering the analysis in the positive direction.

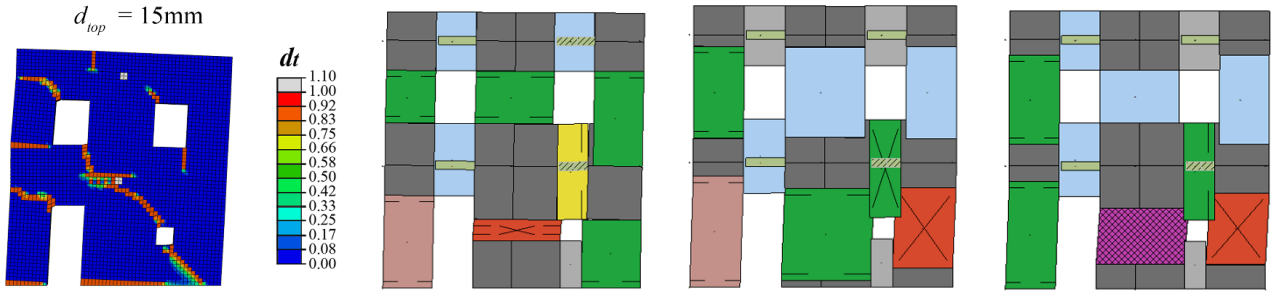

Figure 21 - Configuration BD, analysis in the positive direction: comparison between the damage pattern (d_{top} = 15 mm) resulting from the FE model (a) and the EF models associated to the different criteria for the pier effective height: (b) Augenti (2006); c) Dolce (1991) and d) Lagomarsino et al (2013). See Figure 10 for the meanings of colours and symbols in case of the EF models.

The observation of the damage occurred in the EF models allows to explain the drops of strength observed in the associated global pushover curves. In most of the cases the drops of strength are caused by the reaching of a high state of damage (DL4 or DL5) in element P2. Particularly, P2 tends to assume a very squat geometry due to the presence of the small opening (λ=0.25 according to Augenti (2006),

λ=0.65 according to Lagomarsino et al (2013), λ=0.51 according to Moon et al (2006),), except for the case of the Dolce's proposal (λ=1.03).

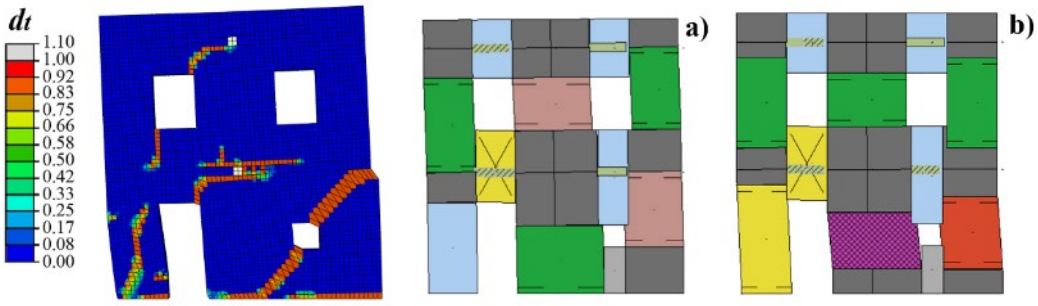

Figure 22 – Configuration BD, analysis in the negative direction: comparison between the damage pattern resulting (d_{top} = 20 mm) from the FE model and the EF models according to: a) Moon et al (2006); b) Lagomarsino et al (2013). See Figure 10 for the meanings of colours and symbols in case of the EF models

Indeed, in all the considered EF models this pier has already reached DL2 (peak of strength) for a top displacement equal to 4 mm. Moreover, a significant state of damage (DL4) in correspondence of d_{top} =15 mm is predicted by the model based on Augenti (2006) (as depicted in Figure 21b) and by the model based on Moon et al (2006), while in the model based on Lagomarsino et al (2013) even the actual collapse (DL5) has already occurred (Figure 21d). Only in the EF model according to Dolce (1991) this pier presents a lower state of damage, being in this case the damage concentrated in the right pier at the ground floor (P3), where DL4 has been reached (Figure 21c).

Accordingly, none of the considered EF models provides a satisfactory description of the actual state of damage. Indeed, in this case the tensile cracks propagate starting from the corners of the small opening as illustrated in Figures 21 and 22 by the FE model. This outcome is even more relevant when looking at the damage pattern emerging from the analyses in the negative direction (Figure 22), even if in this case the global responses provided by the EF models are all quite similar to the curve considered as the reference solution. As an example, the comparison between the damage occurred for a top displacement equal to 20 mm in the FE model and in the EF models based on Lagomarsino et al (2013) and Moon et al (2006) is shown in Figure 22. It is observed that the aspect ratios characterizing P2 are quite similar in these two EF models (Lagomarsino et al (2013) and Moon et al (2006)). In this case, the different behavior exhibited by the panel P2 is ascribable to slight differences in the evolution of the normal stress acting on the element in the two models. Indeed, the range of variation of the normal stress refers to

situations in which the flexural and the shear strength are close, so that small variations in the axial load may lead to different failure modes (shear, flexural or even hybrid), which are characterized by different displacement capacities.

In the FE model the inclination of the tensile crack which develops at the ground floor seems to neglect the presence of the small opening. This suggests that the big masonry portion at the ground floor behaves mostly as a unique pier. On the contrary, when in the EF models the presence of the opening is considered, two different piers are introduced in that part of the wall, so that this type of damage propagation cannot be captured.

4.3. Results on BD configuration: local response

Moving to the comparisons in terms of generalized forces acting on the alignments identified in the wall (Figure 7), the results discussed in the previous sections in the case of configurations B1, B2 and BC are substantially confirmed and even more amplified. This is mainly due to the presence of two adjacent openings with considerably different heights at the ground floor of the wall. From Figure 23a, it is possible to observe that the criterion proposed by Augenti (2006) does not provide good predictions in terms of effective height of the pier at the ground floor, being it too short when compared with the bending moment diagram derived from the FE model. This leads also to a strong overestimation of the shear force acting in this portion of masonry. The same occurs also for the predicted values of bending moment, especially in the case of the pier at the lower storey. Conversely, the criterion suggested by Moon et al (2006) provides a slight better estimate, even also in this case an overestimation of the corresponding shear forces is detected.

On the other hand, considering the EF model based on Lagomarsino et al (2013) (Figure 24), better results in terms of generalized forces are obtained in the initial phase, until the failure of P2, which causes the strong drop of strength observed in the pushover curve. Therefore, rather good predictions in terms of shear force are obtained in correspondence of steps 1 and 2. Nevertheless, when moving to a more advanced nonlinear response (see step 4) , also the predictions of this model are no more consistent

with the results of the FE model. This happens in terms of both generalized forces (Figure 24a/b) and displacements (Figure 24c1/c2).

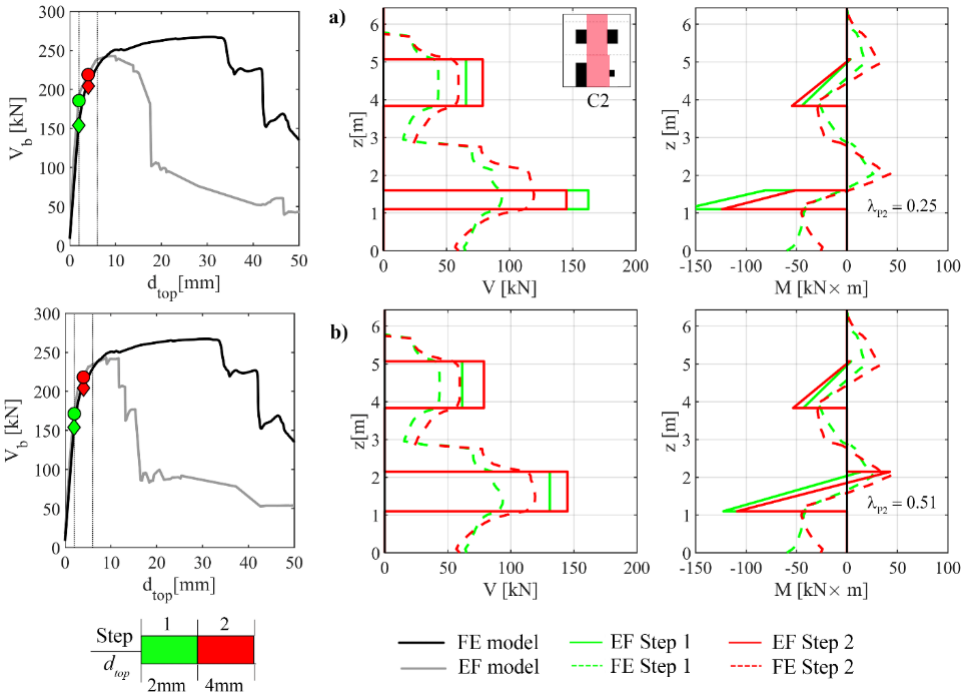

Figure 23 - Configuration BD (positive direction - EF models according to (a) Augenti (2006) and b) Moon et al (2006)) - EF-FE comparison in terms of shear force *V* and bending moment *M* acting on the vertical alignment C2.

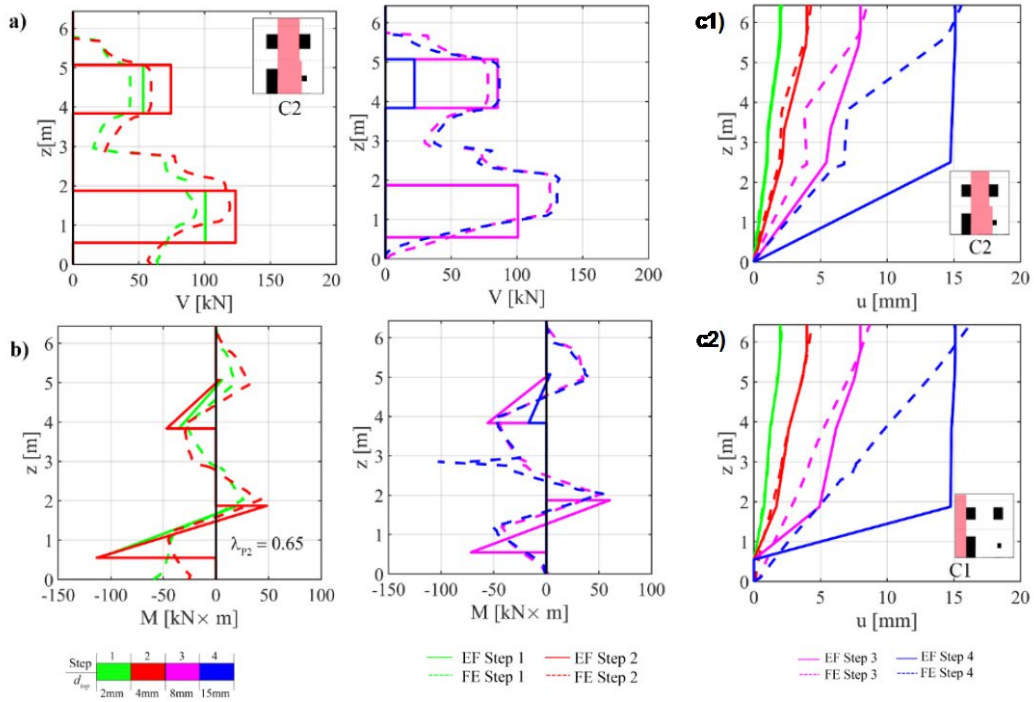

Figure 24 - Configuration BD (positive direction - EF model according to Lagomarsino et al (2013)) - EF-FE comparison in terms of: a) shear force *V*, b) bending moment *M* and c1) horizontal displacements *u* for C2 alignment; c2) horizontal displacements *u* for C1 alignment.

The comparisons in terms of drift values associated to the masonry piers uphold the considerations above expressed (see Figure 25 and Figure 26).

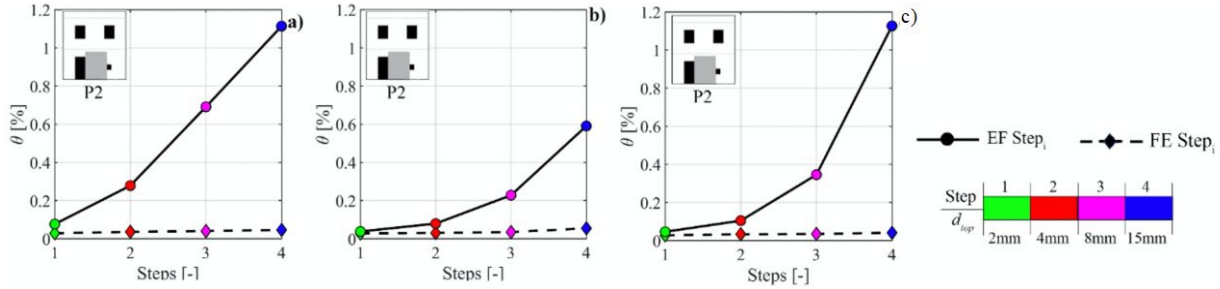

Figure 25 - Configuration BD, analysis in the positive direction: comparison in terms of drift values associated to pier P2 between the FE model and different EF models (a) Augenti (2006); b) Dolce (1991) c) Lagomarsino et al (2013)) for different steps of the analysis.

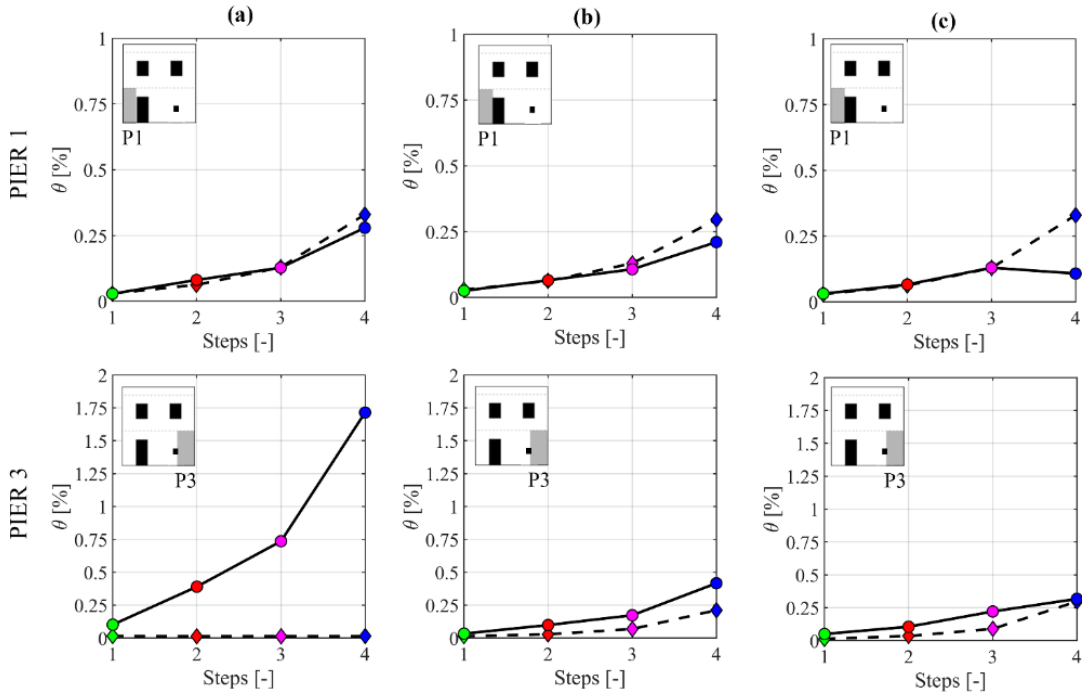

Figure 26 - Configuration BD, analysis in the negative direction: comparison in terms of drift values associated to pier P1 and P3 between the FE model and different EF models (a) Augenti (2006); b) Dolce (1991) c) Moon et al (2006) for different steps of the analysis. See Figure 25 for the legend of colours.

Considering the analyses in the positive direction (Figure 25), indeed, all the examined EF models overestimate the drift associated to pier P2. Only the EF model based on Dolce (1991) provides slightly better predictions in terms of drift, even if still overestimated. The results of the other piers at the ground floor are represented in Figure 26. It can be noted that in case of P1, that is over compressed during the analysis, both the models based on Dolce (1991) and Augenti (2006) provide very satisfactory results. Conversely, when looking at P3, more differences are detected. Both models based on Dolce (1991) and to Moon et al (2006) still provide good results, while a very high overestimation of the actual values of

drift associated to the corresponding masonry portion is observed in case of the model according to Augenti (2006). In this model, indeed, this pier is particularly squat ($\lambda = 0.37$). However, no significant repercussions are present on the associated global pushover curve. This occurs as during the analysis this pier is subjected to a progressive reduction of the compression level, due to the overturning of the wall under the horizontal forces. Therefore, it does not have a significant role in the structural response.

4.4. Directions from the results achieved on BD configuration

The results of configuration BD show that no one of the considered criteria is able to exhaustively capture the actual response activated in the structure neither at global and local scale. In most of the cases the adopted rules lead to particularly stocky piers close to the small opening, strongly affecting the capability of the EF models to reproduce the actual global ductility. This happens especially when considering the analysis in the positive direction, that is associated to the highest scatter of the results with respect to the FE model. In this case, the EF model based on Lagomarsino et al (2013) provides quite good results in terms of generalized forces but only in the initial phase of the analysis, being then the response conditioned by the premature failure of the central pier at the ground floor (P2). The Dolce's criterion, which predicts a higher effective height for the piers adjacent to the small opening, leads to results in terms of generalized forces and drift closer to the reference solution but still not satisfactory in terms of global response. Moreover, even if all the considered EF models are able to capture the concentration of damage at the ground floor, the propagation of the tensile cracks observed in the FE model seems to neglect the presence of the opening. The "No window" model is the only one capable to obtain a better global response. Thus, in this case, this solution is therefore recommended. The above discussed results are summarized in Figure 27 according to the same criteria introduced in Figure 17 (i.e. referring to the worst case scenario and to the alignment C2).

		Moon et al (2006)	Augenti (2006)	Lagomarsino et al (2013)	Dolce (1991)
Global response	V_{max}	L	L	L	M
	$d_{top,n}$	VH	VH	VH	VH
	$k_{s,35}$	H	VH	M	L
Damage pattern	Global failure	Well captured	Well captured	Well captured	Well captured
	Damage in Piers	Not Good	Not Good	Not Good	Not Good
Generalized forces	Shear force	Not Good (Overestimated)	Not Good (Overestimated)	Moderate difference	Moderate difference
	Bending moment	Not Good	Not Good	Moderate difference	Moderate difference
Drift		Not Good (Overestimated)	Not Good (Overestimated)	Not Good (Overestimated)	Not Good (Overestimated)

Figure 27 - Summary of the main outcomes obtained in case of configuration BD.

The application of such recommendation requires to further provide clarifications about what a "sufficiently small" opening means. To this aim, specific parametric analyses with the FE model have been carried out by introducing an opening, centered in a panel, whose dimensions have been then homothetically scaled. The geometric parameters that define each configuration are: the ratio between the length of the opening L_o and the total length of the panel L_p ; the ratio between the height of the opening h_o and the overall height of the panel h_w, which in this case can be assumed representative of an inter-storey height (h_w = 2.85m). The ratio L_o / L_p represents a measure of the reduction of the resisting cross section due to the introduction of the opening. In particular, the configurations illustrated in Figure 28 are associated to L_o/L_p and h_o/h_w ratios respectively equal to 0.05 and 0.08 for P1, 0.07 and 0.13 for P2 and 0.14 and 0.25 for P3; the panel P0 instead is analogous with the one at the base of the BD model. Results refer to the cantilever static scheme and a compression rate (σ/f_m) equal to 4.65%. In particular, from the base shear-top displacement curves (Figure28a) is emerges that configuration P1 almost coincides with P0 and also the P2 is substantially analogous; conversely, configuration P3 highlights appreciable differences both in the pushover curve and in the damage pattern. That clearly indicates how the opening affects the response of the panel, suggesting that it is more appropriate to split it into two piers. The set of parametrical analyses has been then extended by considering also the fixed-fixed boundary condition and other compression rates. By considering all the achieved results, a preliminary indication consists of assuming the "small opening" hypothesis when its height is such that $h_o/h_w < 0.25$

and, at the same time, its width is such that $L_o/L_p < 0.14$ (like configurations P1 and P2). As matter of fact, the dimensions of the opening at the ground floor of wall BD correspond to $h_o/h_w = 0.17$ and L_o/L_p=0.127, respectively.

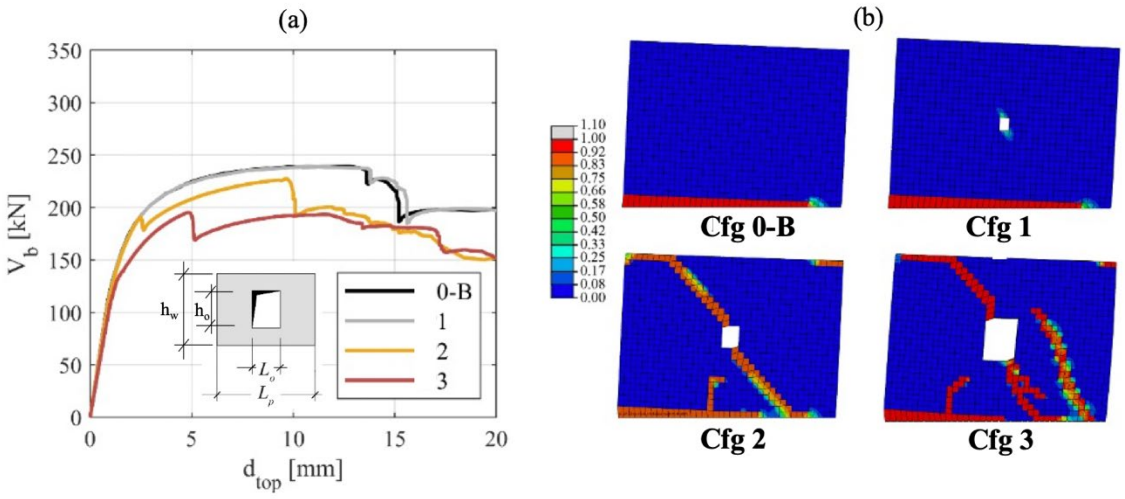

Figure 28 - (a) Base shear - top displacement $V_b - d_{top}$ curves obtained through the analysis of configurations P1, P2 and P3 in case of the compression rate σ/f_m equal to 4.65% and cantilever static scheme; (b) associated tensile damage in correspondence of d_{top} = 10mm.

5. CONCLUSIONS

This paper investigated the reliability of four existing rules for the a priori identification of the geometry of piers in EF models for masonry walls with irregular openings layouts. The critical comparison between continuum FE (used as reference solution) and EF solutions has been carried out in terms of (i) pushover curves, (ii) damage patterns, (iii) generalized forces, and (iv) drift values at scale of single elements. Then, for each rule and for the two main types of irregularity investigated in the paper (i.e. the horizontal irregularity and the presence of small openings), a synthetic judgment on its reliability has been provided, based on both qualitative and quantitative criteria. This synthetic judgment, reported in sections 3.4 and 4.4., aims to collect and transfer all main achieved outcomes into practical recommendations on their use.

Overall, a good effectiveness of the equivalent frame approach in predicting the response assessed by the FE model has been observed, even in presence of irregularities, provided that proper criteria are adopted to identify the geometry of piers.

In the case of horizontal irregularity, results showed that the rules proposed by Lagomarsino et al (2013) and Dolce (1991) already work properly leading to a good match with the reference solution for the estimate of both global and local parameters.

As practical recommendation, the introduction of very squat piers in EF models should be avoided since results testified how their presence may produce unrealistic estimates, if compared with the reference solution provided by the FE model. Indeed, they alter the estimate of stiffness as very big rigid nodes are consequently produced and alter (with a drastic underestimation) the global ductility. The latter effect is particularly relevant since the ultimate displacement capacity of pushover curve is one of parameters most affecting the seismic verification, according to the performance-based approach. In particular, the underestimation of the global ductility in case of very squat piers is due to their premature failure with the consequent sudden softening phase in the pushover curve. This is strictly correlated to the relationship between the height of the panel and the drift estimate.

Finally, the need to define an appropriate modelling strategy has arisen in the case of very small openings. Indeed, the results herein achieved suggest how the most reliable solution consists of neglecting the presence of small wall openings in the EF idealization process. This solution is therefore here recommended. To support the analysts in this choice, a preliminary suggestion, based on ad-hoc parametric analyses, consists of assuming the "small opening" hypothesis when the opening height-to-the wall height ratio is $h_o/h_w < 0.25$ and the opening width-to-the wall width ratio is $L_o/L_p < 0.14$.

As future development of the research, it is worth recalling that the study cases analysed in the paper assume "strong" spandrels (i.e. coupled to r.c. tie beams at each level) with the aim of focusing only to criteria for defining the dimensions of piers. Therefore, the results don't cover issues related to the identification of the spandrel geometry. Thus, in the future, the research effort will be addressed to establish rules for identifying spandrels in presence of vertically misaligned openings or a different number of openings per storey and in the case of walls with weak spandrels.

Acknowledgments: The results were achieved partially (50%) within the national research project ReLUIS-DPC 2019-2021 WP10 – *Contributions to codes developments for URM buildings* (coordinated

by Prof. G. Magenes) and partially (50%) within the project *DETECT-AGING* – "Degradation Effects on sTructural safEty of Cultural heriTAGe constructions through simulation and health monitorING" (Protocol No. 201747Y73L). The ReLUIS project is supported by the funding of the Italian Civil Protection Agency (www.reluis.it) while the *DETECT-AGING* project by the Italian Ministry of Education, University and Research (MIUR).

REFERENCES

Abaqus®, theory manual, version 6.19.

Angiolilli et al. (2021a)The Lattice Discrete Particle Model for the simulation of irregular stone masonry." Journal of Structural Engineering 147.9, 04021123.

Angiolilli, M., Lagomarsino, S., Cattari, S., Degli Abbati, S. (2021b) Seismic fragility assessment of existing masonry buildings in aggregate. Engineering Structures, 247,113218.

Aşıkoğlu A, Vasconcelos G, Louren.o PB, Pant. B (2020) Pushover analysis of unreinforced irregular masonry buildings: lessons from different modeling approaches. *Eng Struct*. https:// doi. org/ 10. 1016/j.engst ruct. 2020. 110830

Asıkoglu A, Vasconcelos G, Lourenço, P.B. (2021) Overview on the Nonlinear Static Procedures and Performance-Based Approach on Modern Unreinforced Masonry Buildings with Structural Irregularity. *Buildings*, 11, 147.

Augenti N (2006) Seismic behavior of irregular masonry walls. *Proceedings of the 1st European Conference on Earthquake Engineering and Seismology*, Geneva, Switzerland.

Augenti N, Parisi F (2010) Learning from Construction Failures due to the 2009 L'Aquila, Italy, Earthquake, *Journal of Performance of Constructed Facilities*, 24(6), pp: 536–555.

Bartoli G. , Betti M., Biagini P., Borghini A., Ciavattone A., Girardi M., Lancioni G., Marra A.M., Ortolani B., Pintucchi B., Salvatori L. (2017) Epistemic Uncertainties in Structural Modeling: A Blind Benchmark for Seismic Assessment of Slender Masonry Towers, J. Perform. Constr. Facil., 2017, 31(5): 04017067

Berti M, Salvatori L, Orlando M, Spinelli P (2017) Unreinforced masonry walls with irregular opening layouts: reliability of equivalent-frame modelling for seismic vulnerability assessment. *Bulletin of Earthquake Engineering,* 15(3), pp:1213-1239.

Berto, L., Saetta, A., Scotta, R., & Vitaliani, R. (2002). An orthotropic damage model for masonry structures. *International Journal for Numerical Methods in Engineering*, 55(2), 127-157.

Beyer K (2012) Peak and residual strengths of brick masonry spandrels, *Engineering Structures*,41, 533-547.

Beyer K., Dazio A (2012) Quasi-static cyclic tests on masonry spandrels, *Earthquake Spectra,* 28(3), pp: 907-929.

Beyer K, Mangalathu S (2013)Review of strength models for masonry spandrels, *Bull Earth Eng*,11,521–542.

Bracchi S, Rota M, Penna A, Magenes G (2015) Consideration of modelling uncertainties in the seismic assessment of masonry buildings by equivalent-frame approach, *Bullettin of Earthquake Engineering*, 13(11), pp: 3423-3448.

Brunelli, A., de Silva, F., Piro, A., Parisi, F., Sica, S., Silvestri, F., Cattari, S. (2021) Numerical simulation of the seismic response and soil–structure interaction for a monitored masonry school building damaged by the 2016 Central Italy earthquake, *Bulletin of Earthquake Engineering*,9(2), 1181-1211.

Calderini C, Cattari S, Lagomarsino S (2009) In-plane strength of unreinforced masonry piers, *Earthquake Engineering and Structural Dynamics*, 38, pp: 243.267

Calderoni B, Cordasco EA, Sandoli A, Onotri V, Tortoriello G (2015), Problematiche di modellazione strutturale di edifici in muratura esistenti soggetti ad azioni sismiche in relazione all'utilizzo di software commerciali. *Proceedings of XVI Convegno ANIDIS*, 13-17 September, L'Aquila, Italy (in Italian).

Calvi GM, Magenes G (1994) Experimental research on response of URM building system. *Proceedings of U.S.-Italy workshop on guidelines for seismic evaluation and rehabilitation of unreinforced masonry buildings*, D. P. Abrams, G. M. Calvi (Eds), State University of New York at Buffalo, NCEER-94-0021, 3-41/57, Pavia.

Castellazzi G, D'Altri AM, de Miranda S, Chiozzi A, Tralli A (2018) Numerical Insights on the Seismic Behavior of a Non-Isolated Historical Masonry Tower, *Bulletin of Earthquake Engineering*, 16 (2), pp: 933–961.

Castellazzi G, Pantò B, Occhipinti G, Talledo DA, Berto L, Camata G (2021) A comparative study on a complex URM building: part II—issues on modelling and seismic analysis through continuum and discrete-macroelement models, *Bulletin of Earthquake Engineering*, 10.1007/s10518-021-01147-4.

Casolo, S., Diana, V., Uva, G. (2016) Influence of soil deformability on the seismic response of a masonry tower, *Bulletin of Earthquake Engineering*, 15(5), 1991–2014.

Cattari S, Lagomarsino S (2013a) Masonry structures, pp.151-200, in: *Developments in the field of displacement based seismic assessment*, Edited by T. Sullivan and Calvi GM, Ed. IUSS Press (PV) and EUCENTRE, pp.524, ISBN:978-88-6198-090-7.

Cattari S, Lagomarsino S (2013b) Analisi nonlineari per la simulazione del danno di un fabbricato in San Felice sul Panaro (Emilia, 2012). *Proceedings of XV Convegno ANIDIS*, 30 June – 4July, Padua, Italy (in Italian).

Cattari S, Chioccariello A, Degée H, Doneaux C, Lagomarsino S, Mordant C (2014) Seismic assessment of masonry buildings from shaking table tests and nonlinear dynamic simulations by the Proper Orthogonal Decomposition (POD). *Proceedings of the 2nd European Conference on Earthquake Engineering and Seismology (ECEES)*, 25-29 August, Istanbul, Turkey.

Cattari S, Magenes G (2021) Benchmarking the software packages to model and assess the seismic response of unreinforced masonry existing buildings through nonlinear static analyses, *Bulletin of Earthquake Engineering*, 10.1007/s10518-021-01078-0

Cattari S, Calderoni B, Caliò I, Camata G, De Miranda S, Magenes G, Milani G, Saetta A (2021a) Nonlinear modelling of the seismic response of masonry structures: review and open issues towards engineering practice, *Bulletin of Earthquake Engineering*, in press.

Cattari, S., Camilletti, D., D'Altri, A. M., & Lagomarsino, S. (2021b). On the use of continuum Finite Element and Equivalent Frame models for the seismic assessment of masonry walls. Journal of Building Engineering, 43, 102519.

CEN (2005) Eurocode 8: Design of structures for earthquake resistance – Part 3: Assessment and retrofitting of buildings. EN1998 – 3, Comité Européen de Normalisation, Brussels.

CNR-DT 212/2013 (2014) Guide for the Probabilistic Assessment of the Seismic Safety of Existing Buildings, National research council of Italy.

D'Altri AM, Sarhosis V, Milani G, Rots J, Cattari S, Lagomarsino S, Sacco E, Tralli A, Castellazzi G, de Miranda S (2019) A review of numerical models for masonry structures, In Woodhead Publishing Series in Civil and Structural Engineering, Numerical Modeling of Masonry and Historical Structures, Woodhead Publishing, 2019, Pages 3-53, https://doi.org/10.1016/B978-0-08-102439-3.00001-4

D'Altri AM, Cannizzaro F, Petracca M, Talledo D (2021) Nonlinear modelling of the seismic response of masonry structures: Calibration strategies, *Bulletin of Earthquake Engineering*, 10.1007/s10518-021-01104-1

De Falco A, Guidetti G, Mori M, Sevieri G (2017) Model uncertainties in seismic analysis of existing masonry buildings: the Equivalent-Frame Model within the Structural Element Models approach. *Proceedings of XVII Convegno ANIDIS*, 17-21 September, Pistoia, Italy (in Italian).

Degli Abbati S, D'Altri AM, Ottonelli D, Castellazzi G, Cattari S, De Miranda S, Lagomarsino S (2019) Seismic assessment of interacting structural units in complex historical masonry constructions by nonlinear static analyses, *Computers & Structures,* 213, pp: 51 – 71.

Degli Abbati S, Morandi P, Cattari S, Spacone E (2021) On the reliability of the equivalent frame models: the case study of permanently monitored Pizzoli's town hall, *Bulletin of Earthquake Engineering*,10.1007/s10518-021-01145-6

Dolce M (1991) Schematizzazione e modellazione degli edifici in muratura soggetti ad azioni sismiche, *L'industria delle costruzioni*, 25 (242), pp. 44-57 (in Italian).

Esposito R., Messali F., Ravenshorst G.J.P., Shipper H.R., Rots J.G. (2019) Seismic assessment of a lab-tested two-storey unreinforced masonry Dutch terraced house, *Bulletin of Earthquake Engineering*,17:4601–4623

Magenes G, Della Fontana A (1998) Simplified non-linear seismic analysis of masonry buildings. *Proc Br Mason Soc* 1:190–195

Moon FL, Yi T, Leon RT, Kahn LF (2006) Recommendations for Seismic Evaluation and Retrofit of Low-Rise URM Structures, *Journal of Structural Engineering*, 132 (5), pp: 663-672.

Lagomarsino S, Penna A, Galasco A, Cattari S (2013) TREMURI program: an equivalent frame model for the nonlinear seismic analysis of masonry buildings, *Engineering structures*, 56, pp: 1787-1799.

Lourenço, P.B. (2002) Computations on historic masonry structures, Progress in Structural Engineering and Mat., 4(3), pp:301-319

Lubliner J, Oliver J, Oller S, Onate E (1989) A Plastic-Damage Model for Concrete, *International Journal of Solids and Structures*, 25, pp: 299–329.

Manzini C, Ottonelli D, Degli Abbati S, Marano C, Cordasco EA (2021) Modelling the seismic response of a 2-storey URM benchmark case study. Comparison among different equivalent frame models, *Bull Earthquake Eng*, 10.1007/s10518-021-01173-2

Marino S, Cattari S, Lagomarsino S, Dizhur D, Ingham J (2019a) Post-earthquake damage simulation of two colonial unreinforced clay brick masonry buildings using the equivalent frame approach *Structures,*19, 212-226.

Marino S, Cattari S, Lagomarsino S (2019b) Are the nonlinear static procedures feasible for the seismic assessment of irregular existing masonry buildings? *Engineering Structures*, 200, 109700.

Marques R, Lourenço PB (2011) Possibilities and comparison of structural component models for the seismic assessment of modern unreinforced masonry buildings, *Computers & Structures*, 89, pp: 2079-2091.

Mercuri, Micaela, et al. "On the collapse of the Medici masonry tower: an integrated discrete-analytical approach." Engineering Structures 246 (2021): 113046.

Milani G (2011) Simple homogenization model for the non-linear analysis of in-plane loaded masonry walls. *Comput Struct* 89:1586–1601

Milani G, Valente M. (2015) Failure analysis of seven masonry churches severely damaged during the 2012 Emilia-Romagna (Italy) earthquake: non-linear dynamic analyses vs conventional static approaches, *Engineering Failure Analysis*,54: 13–56.

Milani, G., Valente, M., Alessandri, C. (2017) 'The Narthex of the Church of the Nativity in Bethlehem: A Non-Linear Finite Element Approach to Predict the Structural Damage', *Computers & Structures,* 207, pp: 3-18.

NTC 2018. Italian Technical Code, Decreto Ministeriale 17/1/2018. Aggiornamento delle Norme tecniche per le costruzioni. Ministry of Infrastructures and Transportation, G.U. n.42 of 20/2/2018 (In Italian).

NZSEE (2017) The Seismic Assessment of Existing Buildings (the Guidelines), Wellington, New Zealand; 2017.

Ottonelli D, Marano C, Manzini C, Calderoni B, Cattari S (2021) A comparative study on a complex URM building. Part I: sensitivity of the seismic response to different modelling options in the equivalent frame models. *Bulletin of Earthquake Engineering*, 10.1007/s10518-021-01128-7

Paquette J, Bruneau M (2003) Pseudo-dynamic testing of unreinforced masonry building with flexible diaphragm, *Journal of Structural Engineering*, 129(6), pp: 708-716.

Pantò, B., Macorini, L., Izzuddin, B. A. (2022). A two-level macroscale continuum description with embedded discontinuities for nonlinear analysis of brick/block masonry. *Computational Mechanics*, 1-26.

Parisi F, Augenti N (2013) Seismic capacity of irregular unreinforced masonry walls with openings, *Earthquake Engineering and Structural Dynamics*, 42, pp: 101–121.

Parisi F, Augenti N, Prota A (2014) Implications of the spandrel type on the lateral behavior of unreinforced masonry walls, *Earthquake Engineering and Structural Dynamics,* 43, pp: 1867–1887.

Parisse F., Cattari S., Marques R., Lourenco P.B., Magenes G. et al. (2021) Benchmarking the seismic assessment of unreinforced masonry buildings from a blind prediction test, *Structures*,31, 982-1005.

Pelà, L., Cervera, M., & Roca, P. (2013). An orthotropic damage model for the analysis of masonry structures. *Construction and Building Materials*, 41, 957-967.

Petracca M, Pel. L, Rossi R, Zaghi S, Camata G, Spacone E (2017) Micro-scale continuous and discrete numerical models for nonlinear analysis of masonry shear walls. *Constr Build Mater*, 149:296–314.

Quagliarini E., Maracchini G., and Clementi F. (2017) Uses and limits of the equivalent frame model on existing unreinforced masonry buildings for assessing their seismic risk: a review, J. Build. Eng.,10, 166–182.

Roca, P., Cervera, M., Griup, G., Pelà, L (2010) Structural analysis of masonry historical constructions. Classical and advanced approaches, Archives of Computational Methods in Engineering, 17 (3), 299-325.

Rossi, M., Cattari, S. & Lagomarsino, S. (2015) Performance-based assessment of the Great Mosque of Algiers. *Bull Earthquake Eng* 13, 369–388.

Siano R, Sepe V, Camata G, Pelà L (2017a) Analysis of the performance in the linear field of Equivalent-Frame Models for Regular and Irregular Masonry Walls, *Engineering Structures,* 145**,** pp: 190–210.

Siano R, Camata G, Sepe V, Spacone E, Roca P, Pelà L (2017b) Finite Elements vs. Equivalent-Frame Models for URM walls' in-plane behavior. *Proceedings of 16th World Conference on Earthquake Engineering*, 9-13 January, Santiago, Chile.

Silva L, Lourenco PB, Milani G (2020) Numerical homogenization-based seismic assessment of an English bond masonry prototype: structural level application. *Earthq Eng Struct Dyn* 49:841–862

STA Data (2017) 3Muri computer program, Release 11.4.0, www.3muri.com

Torres, W., Almazán, J. L., Sandoval, C., & Boroschek, R. (2019). Seismic assessment of irregular masonry macro-elements through a nonlinear framed model: a case study. *Bulletin of Earthquake Engineering*, 17(9), 4937-4960.

Turnšek V, Cačovic F (1971) Some experimental results on the strength of brick masonry walls. *Proceedings of the 2nd international brick masonry conference*, Stoke on Trent, pp. 149-156.

Turnšek V, Sheppard P (1980) The shear and flexural resistance of masonry walls. Some experimental results on the strength of brick masonry walls. *Proceedings of the 2nd international brick masonry conference*, Stoke on Trent, pp. 149-156.

Valente M, Milani G (2016) Non-linear dynamic and static analyses on eight historical masonry towers in the North-East of Italy, *Engineering Structures*, 114, pp: 241–70.

Vanin F, Penna A, Beyer K (2020) A three-dimensional macroelement for modelling the in-plane and outof- plane response of masonry walls. *Earthq Eng Struct Dynam* 49:1365–1387

Yi T, Moon FL, Leon RT, Kahn LF (2006) Lateral load tests on a two-story unreinforced Masonry building, *Journal of Structural Engineering*, 132, pp: 643–652.